

Bachelor of Science in Computer Science & Engineering



A Deep Learning Approach to Predict Autism Spectrum Disorder

by

Faria Zarin Subah

ID: 1504027

Department of Computer Science & Engineering
Chittagong University of Engineering & Technology (CUET)
Chattogram-4349, Bangladesh.

April, 2021

A Deep Learning Approach to Predict Autism Spectrum Disorder



Submitted in partial fulfilment of the requirements for
Degree of Bachelor of Science
in Computer Science & Engineering

by
Faria Zarin Subah
ID: 1504027

Supervised by
Dr. Kaushik Deb
Professor
Department of Computer Science & Engineering

Chittagong University of Engineering & Technology (CUET)
Chattogram-4349, Bangladesh.

April, 2021

The thesis titled '**A Deep Learning Approach to Predict Autism Spectrum Disorder**' submitted by ID: 1504027, Session 2019-2020 has been accepted as satisfactory in fulfilment of the requirement for the degree of Bachelor of Science in Computer Science & Engineering to be awarded by the Chittagong University of Engineering & Technology (CUET).

Board of Examiners

Chairman

Dr. Kaushik Deb
Professor
Department of Computer Science & Engineering
Chittagong University of Engineering & Technology (CUET)

Member (Ex-Officio)

Dr. Md. Mokammel Haque
Professor & Head
Department of Computer Science & Engineering
Chittagong University of Engineering & Technology (CUET)

Member (External)

Dr. Muhammad Ibrahim Khan
Professor
Department of Computer Science & Engineering
Chittagong University of Engineering & Technology (CUET)

Declaration of Originality

This is to certify that I am the sole author of this thesis and that neither any part of this thesis nor the whole of the thesis has been submitted for a degree to any other institution.

I certify that, to the best of my knowledge, my thesis does not infringe upon anyone's copyright nor violate any proprietary rights and that any ideas, techniques, quotations, or any other material from the work of other people included in my thesis, published or otherwise, are fully acknowledged in accordance with the standard referencing practices. I am also aware that if any infringement of anyone's copyright is found, whether intentional or otherwise, I may be subject to legal and disciplinary action determined by Dept. of CSE, CUET.

I hereby assign every rights in the copyright of this thesis work to Dept. of CSE, CUET, who shall be the owner of the copyright of this work and any reproduction or use in any form or by any means whatsoever is prohibited without the consent of Dept. of CSE, CUET.

Signature of the candidate

Date:

Acknowledgements

The journey of writing this thesis towards its completion has only been possible through all the support and supervision that I received from many individuals. This has been a fulfilling experience, both personally and professionally. I would like to convey my thankfulness to a number of people without whom this thesis would have been impossible.

I would like to express my deepest gratitude and honour to my supervisor Dr. Kaushik Deb, Professor, Dept. of CSE, CUET for his constant guidance, endless encouragement and continuous support during my project work. I am thankful for his many critical questions, forcing me to see things from different perspectives. It enabled me to think out of my comfort zone and has enlarged my capabilities to take challenges that I never thought could be done by me.

I would also like to thank the defense committee members, for providing me with their valuable advice, feedback and for appproving my work. I am sincerely grateful to Prof. Md. Mokammel Haque, Head, Dept. of CSE, CUET for his outstanding support throughout my undergraduate education.

I am grateful to my parents for their patience in bearing with me throughout this entire time. Their unconditional love and encouragement has provided support in every aspect of my life.

Abstract

Autism spectrum disorder (ASD) is a complex and degenerative neuro-developmental disorder. Most of the existing methods utilize functional magnetic resonance imaging (fMRI) to detect ASD with a very limited dataset which provides high accuracy but results in poor generalization. To overcome this limitation and to enhance the performance of the automated autism diagnosis model, we propose an ASD detection model using functional connectivity features of resting-state fMRI data. Our proposed model utilizes two commonly used brain atlases, Craddock 200 (CC200) and Automated Anatomical Labelling (AAL), and two rarely used atlases Bootstrap Analysis of Stable Clusters (BASC) and Power. A deep neural network (DNN) classifier is used to perform the classification task. Simulation results indicate that the proposed model outperforms state-of-the-art methods in terms of accuracy. The mean accuracy of the proposed model was 88%, whereas the mean accuracy of the state-of-the-art methods ranged from 67% to 85%. The sensitivity, F1-score, and area under receiver operating characteristic curve (AUC) score of the proposed model were 90%, 87%, and 96%, respectively. Comparative analysis on various scoring strategies show the superiority of BASC atlas over other aforementioned atlases in classifying ASD and control.

Keywords: autism spectrum disorder; resting-state fMRI; predefined brain atlas; ABIDE; functional connectivity; connectivity matrix; functional connectome; deep neural network

Table of Contents

Acknowledgements	iii
Abstract	iv
List of Figures	viii
List of Tables	ix
List of Abbreviations	x
1 Introduction	1
1.1 Introduction	1
1.2 Framework/Design Overview	2
1.3 Difficulties	4
1.4 Applications	4
1.5 Motivation	5
1.6 Contribution of the thesis	6
1.7 Thesis Organization	6
1.8 Conclusion	7
2 Literature Review	8
2.1 Introduction	8
2.2 Overview of Functional Magnetic Resonance Imaging (fMRI) . . .	9
2.3 Related Literature Review	11
2.3.1 Detection using Structural MRI (sMRI)	11
2.3.2 Detection using resting-state functional MRI (rs-MRI) . .	12
2.3.3 Detection in a Combined Approach using both sMRI and rs-fMRI	14
2.4 Conclusion	15
2.4.1 Implementation Challenges	16
3 Methodology	17
3.1 Introduction	17
3.2 Overview of ASD Detection Framework	17
3.3 Detailed Explanation of the ASD Detection Framework	18
3.3.1 Preprocessing	18

3.3.2	Time-series Extraction from ROIs using Brain Atlas	19
3.3.2.1	Selection of Predefined Atlases	20
3.3.2.2	Mean Timeseries Extraction of ROIs from 4D fMRI Brain Volume	21
3.3.3	Building Functional Connectivity Matrix	22
3.3.4	Transforming 2D Functional Connectivity Matrix to 1D Feature Vector	24
3.3.5	Classification	24
3.3.5.1	Hidden Layers and Number of Neurons	25
3.3.5.2	Activation Function	26
3.3.5.3	Optimizer	26
3.3.5.4	Loss Function	27
3.3.5.5	Regularizer	27
3.3.5.6	Batch Size	27
3.3.5.7	Callback Functions	28
3.4	Conclusion	28
4	Results and Discussions	29
4.1	Introduction	29
4.2	Dataset Description	29
4.3	Impact Analysis	30
4.3.1	Social and Environmental Impact	30
4.3.2	Ethical Impact	31
4.4	Evaluation of Autism Spectrum Disorder Detection Framework . .	31
4.5	Evaluation of Performance	33
4.5.1	Performance Evaluation Using Different Atlas	35
4.5.1.1	CC200 Atlas	36
4.5.1.2	Power Atlas	37
4.5.1.3	BASC Atlas	37
4.5.1.4	AAL Atlas	38
4.5.2	Performance Comparison among Atlases	39
4.5.3	Performance Comparison Using BASC Atlas and Single-Site Data	40
4.5.4	Performance Comparison with Machine Learning Methods	41
4.5.5	Performance Comparison with Existing Literature	42
4.6	Conclusion	43
5	Conclusion	44

5.1	Conclusion	44
5.2	Future Work	45

List of Figures

1.1	Block diagram of the ASD detection framework.	3
2.1	Representation of fMRI data.	10
3.1	Steps of the proposed autism spectrum disorder (ASD) detection framework.	18
3.2	Time-series Extraction from 4D fMRI Volume using Brain Parcellation Atlas.	20
3.3	Automated Anatomical Labelling (AAL) atlas.	20
3.4	Bootstrap Analysis of Stable Clusters (BASC) atlas.	21
3.5	Difference between connectomes of random participants belonging to the ASD and control group.	23
3.6	Retrieval of lower triangular part from symmetrical connectivity matrix.	24
3.7	Proposed deep neural network architecture to predict ASD.	25
4.1	Sample of mean time-series data from a random subject using BASC atlas.	31
4.2	Sample of feature vector from a random subject using BASC atlas.	32
4.3	Data partitioning using stratified 5-fold cross-validation.	33
4.4	Confusion Matrix.	34
4.5	Confusion matrix and area under receiver operator characteristic curve (AUC) curve for CC200 atlas using Model-2.	36
4.6	Confusion matrix and area under receiver operator characteristic curve (AUC) curve for Power atlas using Model-2.	37
4.7	Confusion matrix and area under receiver operator characteristic curve (AUC) curve for BASC atlas using Model-2.	38
4.8	Confusion matrix and area under receiver operator characteristic curve (AUC) curve for AAL atlas using Model-2.	39
4.9	Performance comparison among atlases using Model-2.	39
4.10	Performance comparison with different machine learning algorithms.	41

List of Tables

3.1	Steps of CPAC preprocessing pipeline.	19
4.1	Phenotypic information summary of the participants from the ABIDE dataset.	30
4.2	Mean performance evaluation using Craddock 200 (CC200) atlas for different network configurations.	36
4.3	Mean performance evaluation using Power atlas for different network configurations.	37
4.4	Mean performance evaluation using BASC atlas for different network configurations.	38
4.5	Mean performance evaluation using AAL atlas for different network configurations.	38
4.6	Performance comparison using Model-2 and BASC atlas on data obtained from individual screening sites.	40
4.7	Performance comparison with existing literature.	42

List of Abbreviations

- AAL** Automated Anatomical Labeling. 14
- ABIDE** Autism Brain Imaging Data Exchange. 14
- ASD** Autism Spectrum Disorder. 1
- AUC** Area Under the Receiver Operating Characteristic curve. 15
- BASC** Bootstrap Analysis of Stable Clusters. 6, 15
- BOLD** Blood Oxygen Level Dependent. 8
- CC200** Craddock 200. 14
- CPAC** Configurable Pipeline for the Analysis of Connectomes. 14
- CSF** Cerebrospinal Fluid. 8
- DNN** Deep Neural Network. 7
- fMRI** Functional Magnetic Resonance Imaging. 1
- IMPAC** Imaging Psychiatry Challenge. 15
- KNN** K-Nearest Neighbor. 25
- MLP** Multilayer Perceptron. 14
- MRI** Magnetic Resonance Imaging. 1
- MSDL** Multi-subject Dictionary Learning. 15
- PCP** Preprocessed Connectomes Project. 17
- ROI** Regions of Interest. 2
- rs-fMRI** Resting-state Functional Magnetic Resonance Imaging. 2
- TPU** Tensor Processing Unit. 29
- WHO** World Health Organization. 1

Chapter 1

Introduction

1.1 Introduction

Autism spectrum disorder (ASD) is a range of lifelong neurodevelopmental disorders characterized by difficulties in social interaction and communication and by restricted and repetitive patterns of behavior [1]. According to an estimate conducted by the World Health Organization (WHO), 1 in 160 children suffers from ASD worldwide [2]. It is associated with an array of behavioral symptoms which may take a drastic form if the diagnosis is delayed [3, 4]. Although symptoms are prevalent during infancy, diagnosis is delayed in most cases. It is because the current diagnostic procedure of ASD is purely subjective and interview-based that requires the physician to go through a child's developmental history and behavior [5, 6]. Though these methods are quite accurate, they are undoubtedly exhaustive, extensive, and also require professional expertise that might not be available at many health institutions.

Nevertheless, during the past several decades, research work focusing on magnetic resonance imaging (MRI) and functional magnetic resonance imaging (fMRI) using machine learning and deep learning techniques are on the rise to detect brain anomalies that would be an indicator for autism. Such automated approaches would decrease subjectivity and improve diagnostic reproducibility and availability. It would also play a substantial role in ensuring early diagnosis. However, very few studies related to detecting ASD using MRI data and deep learning technology has taken into consideration, the entire set of a demographically heterogeneous clinical population of ASD subjects comprising a wide age range and achieved high accuracy. This results in poor generalization producing unreliable

results.

The overview of functional MRI data and the proposed framework for detecting ASD using derived features from resting-state functional magnetic resonance imaging (rs-fMRI) data is provided in this section along with the challenges encountered in the process. This chapter also discusses the motivation, application and contribution of the proposed methodology in autism spectrum disorder detection.

1.2 Framework/Design Overview

In the neuroimaging field, use of resting-state fMRI data in detecting neurocognitive disorder is evolving at a very high pace. Studies mostly rely on access to raw image data. However, sharing patient images can be troublesome due to patient identifiability concerns. Besides, raw fMRI data takes up a huge amount of processing time and might suffer from overfitting due to its high dimensionality.

Taking into account the above issues, we have proposed a deep learning approach to detect autism spectrum disorder from functional connectomes which can be derived from rs- fMRI data. A functional connectome can be defined as a functional connectivity matrix that measures the correlation between a set of individual brain ROIs (regions of interest) as defined by a brain atlas. It characterizes the network structure of the brain and can be extracted from functional interactions in rs-fMRI data. An individual subjects' behaviour, cognition, and psychiatric health are characterized by using the corresponding weights of the functional connectome [7].

The block diagram of our proposed framework is represented in Figure 1.1:

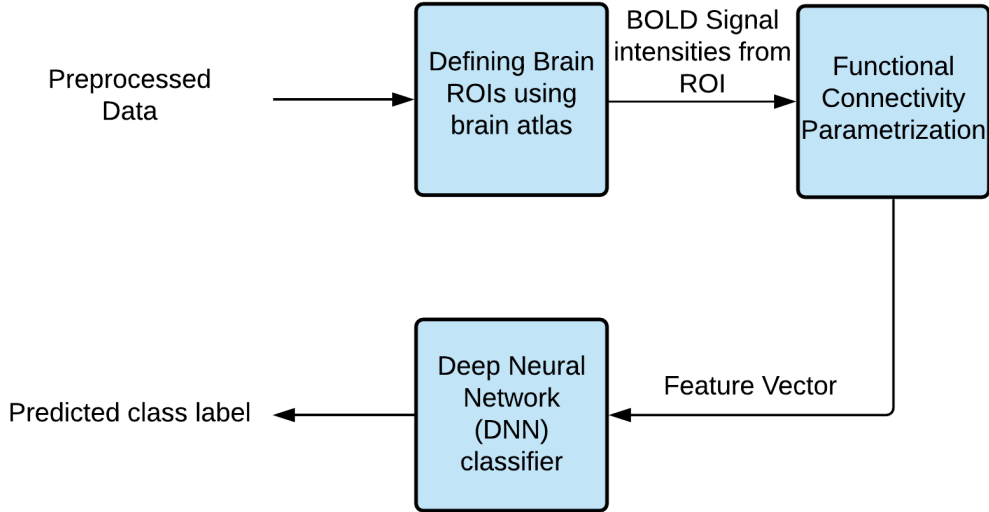


Figure 1.1: Block diagram of the ASD detection framework.

Our functional connectivity feature or functional connectome based ASD prediction framework comprises the following main steps:

1. **Preprocessed Data:** Preprocessed rs-fMRI dataset are directly obtained from the CPAC preprocessing pipeline. Preprocessing is required for nuisance signal removal, slice time correction, motion correction, skull stripping, etc.
2. **Defining brain ROIs using brain atlas:** Specific brain regions of interest (ROIs) are identified using pre-defined brain atlases. Time-series signals or BOLD signal intensities are extracted only from those regions that are defined by the respective brain atlas.
3. **Functional Connectivity Parametrization:** Functional interactions from time-series signals are obtained from these ROIs and quantified using tangent space connectivity measure to obtain a functional connectome or functional connectivity matrix.
4. **Classification:** Functional connectomes are flattened to produce one-dimensional

feature vectors and provided as input to a deep neural network classifier which predicts the class label i.e. autism or control.

1.3 Difficulties

In this study, we worked with more than 800 subjects' data (including ASD and control), collected from 17 different international brain imaging laboratories worldwide belonging to an age range of 7-64 years. The heterogeneity and complexity of such a dataset pose various difficulties. The major difficulties are enlisted below:

1. **Reduced accuracy with larger dataset:** Many potential sources of uncontrolled variation exist across studies and sites due to MRI acquisition protocols (such as scanner type, imaging sequence), participant instructions (such as eyes open vs closed), recruitment strategies (such as age group, IQ range, level of impairment, treatment history and acceptable comorbidities) in [8]. Such variation affects computer-aided diagnosis and provides low accuracy.
2. **Poor generalization with smaller dataset:** An accuracy above 0.9 is obtained considering only a dozen subjects in [9] and accuracy deteriorates consequently when a larger dataset is considered. Thus, high accuracy can be achieved very conveniently when using data from a single site. In contrast, such a procedure would not generalize the problem efficiently.

Hence, obtaining a reliable and fair accuracy using a heterogeneous dataset comprising a large number of participants/subjects is quite a challenge.

1.4 Applications

The entire procedure of autism detection prevailing at present comprises a wide spectrum of developmental monitoring, screening, comprehensive developmental evaluation including parents interview, questionnaire and so on. This is a very

complicated and comprehensive method. Again, the absence of an objective medical test like a blood test, PET scan, EEG, CT scan, etc is also responsible for a delayed autism diagnosis. The successful implementation of deep learning in detecting ASD from brain fMRI data may be used for a wide range of application:

1. Assistive technology for neuroscientists enabling them to obtain valuable insights regarding autism spectrum disorder.
2. Visual evaluation of the functional characteristics and properties of the autistic brain.
3. Identifying neural activation patterns responsible for autism and associating those patterns with physiological and psychological features would result in a more reliable diagnosis.
4. By examining the contrast of rs-fMRI data of autistic and control brain the underlying neural or biological basis of autism disorder can be unveiled and established.

1.5 Motivation

To compete with the advancement of technologies in the neuroimaging field, there exists a scope for improving the existing methods related to diagnosing neuropsychiatric disorders utilizing functional MRI to produce results with more accuracy. The primary motivation working behind this thesis can be listed as below:

1. **To overcome existing limitations:** Most studies suffered from low accuracy and huge training time problems using more than 800 subjects [10]. Our goal is to achieve superior accuracy reducing the amount of training time thus alleviating the limitations of previous work.
2. **To introduce automated ASD diagnosis:** The traditional procedure for ASD diagnosis, comprising an extensive battery of behavioural tests is less available than desired. Many clinics may not have such facilities and

experts capable of conducting such assessments. Automated MRI based diagnosis can serve as a fruitful solution in this case.

3. **To reduce subjectivity in the field of diagnosis:** Automated computer-aided diagnosis can be provided instead of a purely subjective and interview-based diagnosis. It can also act as a supplement to the current diagnostic system.
4. **Early detection of autism:** Early autism diagnosis is indispensable to prevent the condition from intensifying further. This can be provided by MRI-based diagnosis. It is a pain-free, non-invasive (requiring no medication, injection or anaesthesia) diagnostic tool without side effects suitable for any age allowing early diagnosis.

1.6 Contribution of the thesis

Thesis or research works are conducted to fulfill a particular array of goals either by defining a new methodology or by alleviating the limitations of the existing ones. In this thesis, the prime objective is to focus on improving the accuracy of ASD detection using only rs-MRI data while reducing training time. The primary contributions of this thesis are as follow:

1. Achieved a maximum accuracy of 88% using only resting-state functional MRI (rs-fMRI) time-series data by the proposed scratch deep neural network model.
2. Reached the conclusion that the rarely used Bootstrap Analysis of Stable Clusters (BASC) atlas using 122 ROIs yield a higher predictive power than other predefined atlases from comparative analysis.

1.7 Thesis Organization

The remaining chapters are organized as follow:

- Chapter 2 gives a summary of previous research works, their contributions and limitations in ASD detection using MRI data.
- Chapter 3 describes the proposed methodology to detect ASD in detail with visual representations wherever possible. In the proposed architecture, four different brain atlases were used one at a time to perform the prediction task. The classifier used is a deep neural network or DNN.
- Chapter 4 describes the working dataset and the performance analysis for the proposed method.
- Chapter 5 contains the overall summary of this thesis, its limitations and future recommendations as well.

1.8 Conclusion

In this chapter, a brief overview of our research work has been discussed. A summary of the proposed framework, as well as the motivation behind this thesis and its applications, have been represented. The research contributions along with the challenges faced are also stated. In the next chapter, background, literature reviews and the current state of the problem shall be provided.

Chapter 2

Literature Review

2.1 Introduction

Recently, with the advancement of technology, a large cohort of studies are considering an automated computer-aided diagnosis of autism [11, 12, 13] and also developing interactive tools to aid in the rehabilitation and treatment of autistic patients [14, 15, 16]. Such automated approaches would decrease subjectivity and improve diagnostic reproducibility and availability. It would also play a substantial role in ensuring early diagnosis.

The two most fundamental and widely used MRI image types are – 1) Structural (sometimes called anatomical) and 2) Functional images. A structural MRI image is a three-dimensional image that contains information about the anatomy of the brain like grey/white matter volume, CSF (cerebrospinal fluid), etc. While functional MRI scans produce a set of 3D images recorded over time and measure a signal (most commonly, the BOLD signal) that is related to neural activity. Magnetic resonance imaging (MRI) can be used to detect various neuropsychiatric and neurodegenerative disorders, such as schizophrenia [17, 18, 19, 20], dementia, depression [21], autism [22, 23, 24, 25], ADHD [26], Alzheimer's [27, 28], etc., by observing anatomical patterns of the brain using structural MRI data or by connecting changes in the brains' functional architecture to psychiatric health conditions using functional MRI data.

Since this research work deals only with autism detection, the focus of this chapter is to present a comprehensive literature review of various ASD detection approaches using either structural and functional MRI and a combined approach

that includes both. In this regard, functional MRI indicates only resting-state functional MRI i.e, rs-fMRI. Through providing a summary of previous related studies, this part of the thesis discusses methods applied by different researchers, their performance evaluation, challenges faced and limitations. A brief overview of fMRI is also represented in the following section in order to familiarize with the type of data generated by fMRI scans.

2.2 Overview of Functional Magnetic Resonance Imaging (fMRI)

A human brain can be defined as a complex agglomeration of interconnected systems comprising a large number of regions conducting various functions. Although some structural regions may not possess unmediated and direct connection, they are associated globally to process numerous varieties of information as a whole [29]. Magnetic Resonance Imaging or MRI is a radiological technique used to visualize 3D images representing the anatomical and physiological processes of the brain [30]. Functional MRI or fMRI is a special type of MRI that measures spontaneous fluctuations in brain activity by detecting changes related to blood using the BOLD signal while the subject performs an explicit task such as, tapping his/her finger, moving his/her arm, squeezing a ball, looking at a picture, etc.

BOLD is the abbreviation for Blood Oxygen Level Dependent. It is a time-varying signal modulated by changes in the oxygen content of the blood that enables in identifying active brain areas while performing a task. Neurons in the active brain areas that respond in carrying out the task tend to receive a high amount of oxygenated blood which in turn increases the BOLD signal intensity measured in that area. A human brain is a 3D object and fMRI takes picture of it by making a series of slices and within each slice there exists a 2D picture of neuronal activities going on in that slice. Such 3D images are taken at different timepoints recording the change of activities across time. Thus a raw fMRI data

of a single subject is 4D where the 4th dimension represents time.

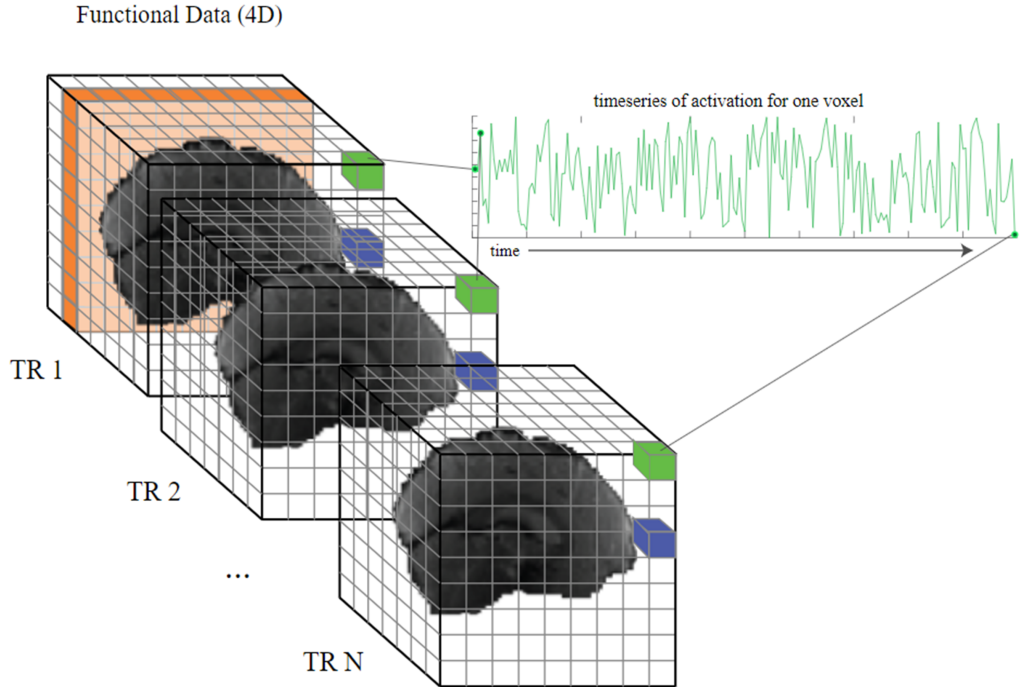


Figure 2.1: Representation of fMRI data.

Some basic terminologies related to fMRI data are discussed:

- **Volume:** The entire three-dimensional pixel grid covering the space that was imaged by the MRI scanner. The volume is composed of many smaller voxels. Functional data has a volume for each time point of the experiment.
- **Voxel:** A three-dimensional pixel and the basic unit of spatial measurement in MRI (represented by green and blue cubes in Figure 2.1).
- **Slice:** All of the voxels in a 2D plane taken from the 3D volume (shown in orange in Figure 2.1).
- **TR:** Abbreviation for repetition time. The basic unit of time in functional MRI. One volume is scanned every TR.

Resting-state fMRI (rs-fMRI) is a special type of f-MRI technique that performs

brain mapping to evaluate regional interactions occurring in a task-negative state i.e when an explicit task is not being performed. In this case, a subject lies in the MRI scanner without thinking or doing anything in particular according to [31]. The data utilized in this study is resting-state fMRI data which is devoid of the complications and difficulties associated with task-evoked or fMRI data.

2.3 Related Literature Review

2.3.1 Detection using Structural MRI (sMRI)

Structural MRI studies emphasise upon volumetric and morphometric analyses to detect abnormal brain anatomy.

A voxel-based morphometry analysis was performed by Riddle et al. in [32] and it was observed that the grey matter volumes, the left anterior superior temporal gyrus and the total brain volume are enlarged in ASD children by 1-2% approximately.

Besides, Aylward et al. in [33] measured total brain volumes and head circumference from 1.5-mm coronal MRI scans in 67 autistic subjects and 83 healthy community volunteers within the age range of 8-46 years but observed no brain volumetric differences between ASD and control subjects aged above 12. Thus, total brain volume cannot be treated as a biomarker to detect ASD comprising all age range.

Palmen et al. in [34] acquired brain MRI scans from 21 high-functioning autistic subjects and 21 control subjects belonging to 7-15 years. This study concluded that high-functioning autistic subjects showed an enlargement of grey-matter volume. No increase in white-matter and cerebellar volume was observed. However, Courchesne et al. in [35] also reported an increase in grey matter volume, particularly in the temporal lobes in autism.

On the contrary, an increased white matter and reduced cerebral cortex and hippocampusamygdala were found in the autistic brain by Herbert et al. [36] performing MRI-based morphometric analysis on all-male subjects that included 17 autistic and 15 control ones between 7-11 years of age. Conversely, Jou et al. in [37] observed decreased central white matter volume in autistic subjects performing experiments using MRI data obtained at 1.5-T and analyzed via BRAINS2 software from 23 autistic and 23 matched control boys.

Thus, all the previous works of literature stated above failed to reach strong conclusions regarding volumetric changes using only structural MRI data and presented inconsistent findings regarding grey and white matter volumes in autism and control brain. The use of small sample size, limited age range and including only male subjects can be regarded as a limitation.

However, Kong et al. in [38] presented a promising study and a unique methodology to solve the classification problem using structural information from MRI data. An individual brain network was constructed for each subject and connectivity features were extracted between each pair of ROIs. Then, these features were ranked by Fisher score computation. The top 3000 features were provided as input to a deep neural network classifier. Results showed a very high accuracy of 90.39% and an AUC score of 97.38% using 182 subjects from a single site. However, such low number of participants might result in poor generalization.

2.3.2 Detection using resting-state functional MRI (rs-MRI)

Biswal et al. in [39] discovered that different brain regions actively interact with each other while a subject was at rest i.e, not performing any cognitive task. Then onwards, rsfMRI has evolved as a noteworthy tool to explore brain networks by investigating local and global connectivity patterns. At present, it is

recognized as one of the most efficient methods to detect different brain disorders.

Nielson et al. in [40] used whole-brain point-to-point functional connectivity including rsfMRI data obtained from the ABIDE (Autism Brain Imaging Data Exchange) dataset comprising 964 subjects collected from 16 different international sites. Raw image data were preprocessed in MATLAB using SP8. After preprocessing, mean BOLD signals for each subject were extracted from 7266 grey matter ROIs. A 7266×7266 association matrix representing functional connectivity between every ROI pairs was computed from Pearson correlation coefficients for every subject. Each ROI pairs were defined as a connection. Connections, categorized into several bins and a general linear model classifier was fitted on bins containing connections. Very low accuracy of merely 60% was achieved for whole-brain classification.

Heinsfeld et al. [10] applied deep learning algorithm combining a multilayered perceptron (MLP) along with the unsupervised training of two stacked denoising autoencoders. Here, preprocessed data were downloaded from the CPAC pre-processing pipeline. Mean time series was extracted using the CC200 ROI atlas for each subject. Time series for each subject was converted to a 200×200 connectivity matrix using Pearson correlation coefficient which was further reduced to a feature vector comprising 19,900 features by removing the upper half triangular part and principal diagonal from the connectivity matrix. The remaining lower triangular part was flattened to a feature vector containing derived features from MRI image data and finally fed to the deep learning classifier. 70% mean classification accuracy was obtained and brain areas that contributed the most to classifying ASD and control were identified. However, took a huge training time (over 32 hours).

Eslami et al. [41] proposed ASD-Diagnet, a framework for detecting ASD using only rs-fMRI data. A combined learning procedure using an autoencoder and a single layered perceptron (SLP) was used which resulted in a greater quality of extracted features and optimized parameters for the model in [41]. Furthermore,

to increase the number of training subjects a data augmentation strategy, based on linear interpolation on available feature vectors was implemented. However, this strategy could improve accuracy only by 1% and presented a mean classification accuracy of 70.1%. It also gave an enormous advantage in the case of training time (40 minutes).

A deep multimodal model able to learn a joint representation from 2 types of connectomic data, (i) ROI time series activation map and (ii) fMRI \times ROI activation map offered by rsfMRI scans was proposed by Tang et al. in [42]. A 3D Resnet and MLP classifier were used in the classification process. This approach displayed 74% classification accuracy, 95% recall, 0.805 F1-score and proved an overall superior performance using a single type of functional data.

2.3.3 Detection in a Combined Approach using both sMRI and rs-fMRI

A fusion approach using both structural and functional data have also been applied in the ASD and control classification pipeline. Each element in a functional data-based connectivity matrix imparts information regarding correlation coefficients of averaged BOLD signal from ROI pairs. On the contrary, elements in a structural data-based connectivity matrix provide information regarding cortical grey matter volumes.

Rakić et al. [43] proposed such a combined approach using 817 cases from the ABIDE dataset. Steps of the framework included preprocessing structural (using FreeSurfer software) and functional (CPAC preprocessing pipeline) data, feature extraction (using AAL and CC200 parcellation for functional and Destrieux atlas for structural data) and representation using connectivity matrices. Fisher score was computed for feature reduction and finally, data classification was performed by an ensemble of autoencoders and MLP $85.06 \pm 3.52\%$ classification accuracy

was obtained using an ensemble of classifiers.

The research conducted by Mellema et al. in [44] compared classification performance via 12 classifiers using more than 900 subjects from the IMPAC database. The derived structural and functional features were obtained directly from IMPAC. The 12 classifiers included 6 nonlinear shallow models, 3 linear shallow models and 3 deep learning model. For structural data, the Desikan-Killiany gyrus atlas was used to extract ROIs. While functional data used 7 different predefined atlases namely: BASC-64, BASC-122, BASC-197, Craddock which defines 249 ROIs, Harvard-Oxford containing 69 ROIs, MSDL with 39 ROIs and the Power Atlas comprising 264 ROIs. For connectivity matrix parametrization, tangent space embedding was used. The dense FeedFWD network was found to be the best model achieving 0.80 AUC with the fusion of anatomical data and functional data from BASC atlas comprising 122 ROIs.

2.4 Conclusion

In this chapter, a detailed literature review of related works has been discussed. For convenience, this discussion was divided into three categories depending on the proposed approach and data type used. From the above discussion, it is evident that structural MRI data approaches mainly focused on determining common brain patterns between ASD vs control rather than solving the inherent classification problem. Structural data-based studies also resulted in inconsistent findings. On the contrary, combined approaches resulted in quite satisfactory results but it requires the availability of both types of MRI data for each patient which might be problematic in a practical scenario. Thus, in this study, we will mainly focus on improving the existing classification accuracy using only rs-fMRI data. An elaborate description of the proposed methodology will be discussed in the upcoming chapter.

2.4.1 Implementation Challenges

The implementation of this research work posed a number of challenges which are stated:

- **Optimizing a massive number of parameters:** In this thesis, we used a deep neural network classifier. Such deep learning-based classifiers require optimizing a massive amount of hyperparameters such as hidden layer configuration, neurons per layer, regularization technique, activation function, amount of dropout, etc. Especially high dimensional dataset and limited training samples (which is the case in the neuroscientific community) make the task of hyperparameter searching, optimization and overfitting prevention even more strenuous.
- **Difficulties in detection without demographic information:** Various studies used the demographic information of the subjects such as age, IQ, and handedness in their methods or selected subsets of subjects with specific attributes in their analysis in [41] However, using only fMRI data without taking into account other phenotypic and demographic information would ensure an independent and unbiased decision in diagnosis. Although, the presence of such demographic information would result in higher predictive power. But, our objective is to depend solely on fMRI data to avoid biases, which is a more challenging task.

Chapter 3

Methodology

3.1 Introduction

The function of rs-fMRI scans is to study neuronal activities across time by tracking changes in the BOLD signal while the subject is in a task-negative state. Thus, raw functional images are 4D where each dimension represents the height, width, depth/number of brain slices and time of repetition of each subject/sample.

However, in this research, we will not use fMRI image data rather we will represent fMRI scans as mean time-series data from particular ROIs. These specific ROIs are selected using a functionally parcellated brain atlas. Each of these atlases use different approaches to segment the entire brain into several ROIs. The various steps of our proposed methodology are discussed in this chapter in detail.

3.2 Overview of ASD Detection Framework

Figure 3.1 represents the basic steps of the proposed autism detection framework. Preprocessed rs-fMRI data of the ABIDE dataset are obtained from the Preprocessed Connectome Project (PCP). The CPAC preprocessing pipeline is applied for nuisance signal removal and attaining quality criteria. After that, certain brain areas of interest are considered using brain atlases. These brain atlases serve as a mask that extracts signals of certain predefined ROIs from the preprocessed dataset. A connectivity matrix is created using tangent space embedding that provides information about the intensity of correlation between each ROI pairs. Finally, the connectivity matrix is collapsed to form a 1D vector removing

redundant elements. This feature vector is provided as input to the deep learning classifier. During training, the feature vector along with the corresponding label of each sample (i.e, either autism or control) are provided as input to the DNN classifier. Using this trained classifier, testing is executed where the labels of each test sample were determined by the classifier.

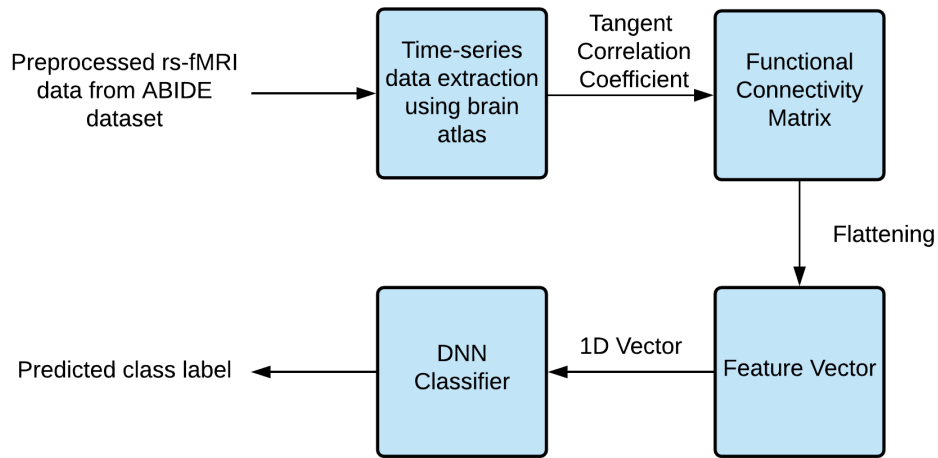


Figure 3.1: Steps of the proposed autism spectrum disorder (ASD) detection framework.

3.3 Detailed Explanation of the ASD Detection Framework

The explanation of each steps conducted in the entire process of ASD detection is represented in the following subsections along with their implementation details.

3.3.1 Preprocessing

The preprocessed fMRI dataset of the ABIDE repository [45, 46] was collected from the preprocessed connectome project (PCP) [47]. The configurable pipeline for the analysis of connectomes (CPAC) preprocessing pipeline was used, which included slice timing correction, motion correction, intensity normalization, nuisance signal removals, such as respiration, heartbeat, low-frequency scanner drifts, global mean signal regression, head motion, etc. The preprocessed data were

band-pass filtered (0.01–0.1 Hz) and spatially registered to MNI152 template space. Table 3.1 contains an overview of the preprocessing steps included in the CPAC pipeline.

Table 3.1: Steps of CPAC preprocessing pipeline.

Steps	CPAC
Regressor	
Motion	24-param
Tissue signals	CompCor (5 PCs)
Low-frequency drifts	Linear and quadratic trends
Registration from original to MNI152	
Functional to Anatomical transform	boundary-rigid body (BBR)
Anatomical to Standard transform	ANTs

Detailed information regarding algorithms, strategies, parameters used, and software implemented can be obtained from [48].

3.3.2 Time-series Extraction from ROIs using Brain Atlas

The accuracy of ASD and control classification largely depends on the brain atlas used to extract specific regions of interest (ROI) from whole-brain fMRI volumes. The hypothesis is to use a parcellation atlas, either by data-driven method or from the predefined ones such that, the selected ROIs contain regions comprising the most discriminative features between an autistic brain and control brain. In this study, we consider four standard predefined brain atlases among which three are functional (BASC, Power, CC200) and one is structural (AAL). A pictorial representation of time-series extraction from fMRI volume using brain atlas is visualized in Figure 3.2.

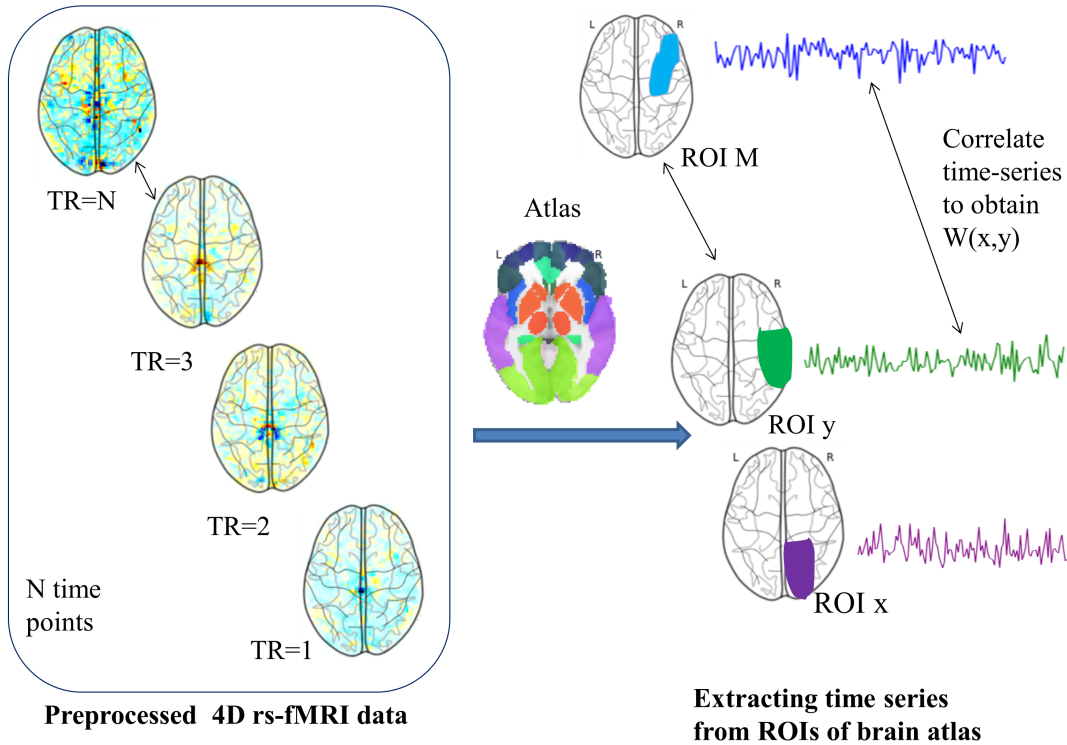


Figure 3.2: Time-series Extraction from 4D fMRI Volume using Brain Parcellation Atlas.

3.3.2.1 Selection of Predefined Atlases

- **AAL – Automated Anatomical Labelling:**

It is a structural atlas comprising 116 ROIs defined from the anatomy of a reference object in [49]. The 116 regions are defined by AAL atlas along the three anatomical planes (Axial, Sagittal and Coronal) as shown in Figure 3.3 for visualization purpose where ROIs are represented in continuous colours.

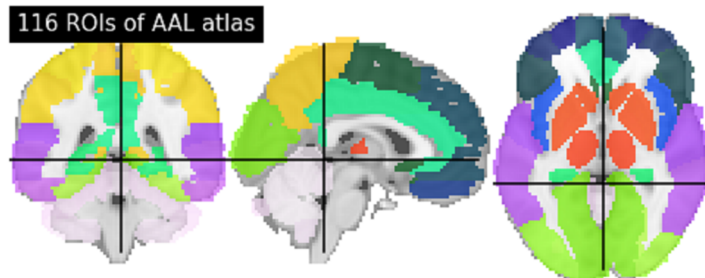


Figure 3.3: Automated Anatomical Labelling (AAL) atlas.

- **BASC – Bootstrap Analysis of Stable Clusters:**

This multiscale functional brain parcellation atlas was generated from rs-fMRI images from about 200 young healthy subjects using a method called bootstrap analysis of stable clusters in [50]. It consists of a different number of ROIs 36, 64, 122, 197, 325, 444. BASC atlas with 122 ROIs is utilized in this study. The visual representation of this atlas is shown in Figure 3.4 using continuous colours to represent ROIs.

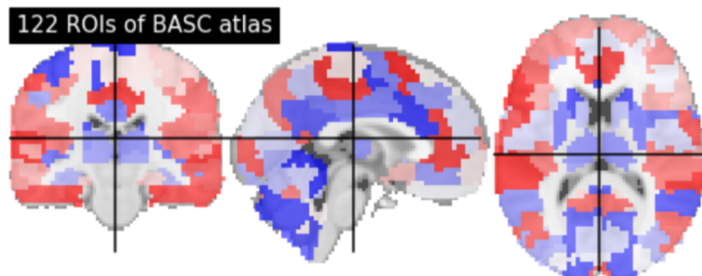


Figure 3.4: Bootstrap Analysis of Stable Clusters (BASC) atlas.

- **CC200—Craddock 200:**

The CC200 functional brain parcellation atlas was generated by normalized cut spectral clustering of the entire brain into 200 spatially-constrained regions of homogeneous functional activity by Craddock et al. in [51].

- **Power:**

Power atlas comprising 264 ROIs were defined by local graph-connectivity by Power et al. in [52].

All the brain images used in this section were generated by the Nilearn Python library using the plotting function. Nilearn is a python module for easy and fast statistical learning on neuroimaging data which provides tools and functions to enable versatile analyses of brain volumes in [53].

3.3.2.2 Mean Timeseries Extraction of ROIs from 4D fMRI Brain Volume

A single fMRI scan is a 4D time-series including three spatial dimensions and time. In order to extract and transform meaningful features from such complicated multidimensional data in a structured way and to store it in a convenient

format, certain pre-defined regions of interests (ROIs) are considered.

In other words, instead of working with the entire time series obtained from every brain voxels directly, we consider certain brain regions comprising several voxels and extract mean time-series signals from voxels enclosed within those regions. To accomplish this, we use a brain atlas where the brain regions or the ROIs are already defined. Applying a brain atlas on 4D fMRI scans can be imagined as overlaying a series of 3D grids that act like a mask and selects which cubes or voxels to sample from at every time point.

Thus, original 4D fMRI data of a single subject with dimensions (H, W, D, T) gets transformed to 2D data with dimensions (T, N) where H, W, D, T represents height, width, depth or number of slices, time points of the image volume and number of ROIs, respectively. Now, this 2D data can form a TxN matrix where each row represents time points and each column represent features derived from rs-fMRI data.

However, the whole process of extracting mean time-series signals applying brain atlas on preprocessed rs-fMRI data requires a huge amount of memory space. Due to hardware and memory constraints, we utilized pre-extracted time-series data. In this study, mean time-series signals containing CC200 and AAL defined ROIs were obtained directly from PCP [48], and those containing BASC and Power atlas defined ROIs were collected from [54]. Thus, the (T, N) dimension in our study was (196, 200), (196, 116), (196, 122), and (196, 264) for CC200, AAL, BASC, and Power, respectively, since scans were generated for 196 time points in each case.

3.3.3 Building Functional Connectivity Matrix

The (T, N) dimensional data were then transformed into a functional connectivity matrix or a connectome with dimensions (N, N). A functional connectome can be defined as a connectivity matrix that measures the correlation between a set

of individual brain ROIs as defined by the respective brain atlas. In this case, dimensions became (200, 200), (116, 116), (122, 122), and (264, 264) for CC200, AAL, BASC, and Power atlases, respectively.

To build functional connectomes, tangent embedded parametrization of the default Ledoit-Wolf regularized covariance estimator was implemented using the Nilearn library [53]. Tangent space embedding uses both correlations and partial correlations to capture reproducible connectivity patterns at the group-level and models individual connectivities as deviations from the mean [55]. Functional connectivity matrices are represented in Figure 3.5 as an embedded connectome to visualize the striking differences between functional connectivity among brain regions from a random autistic and control sample.

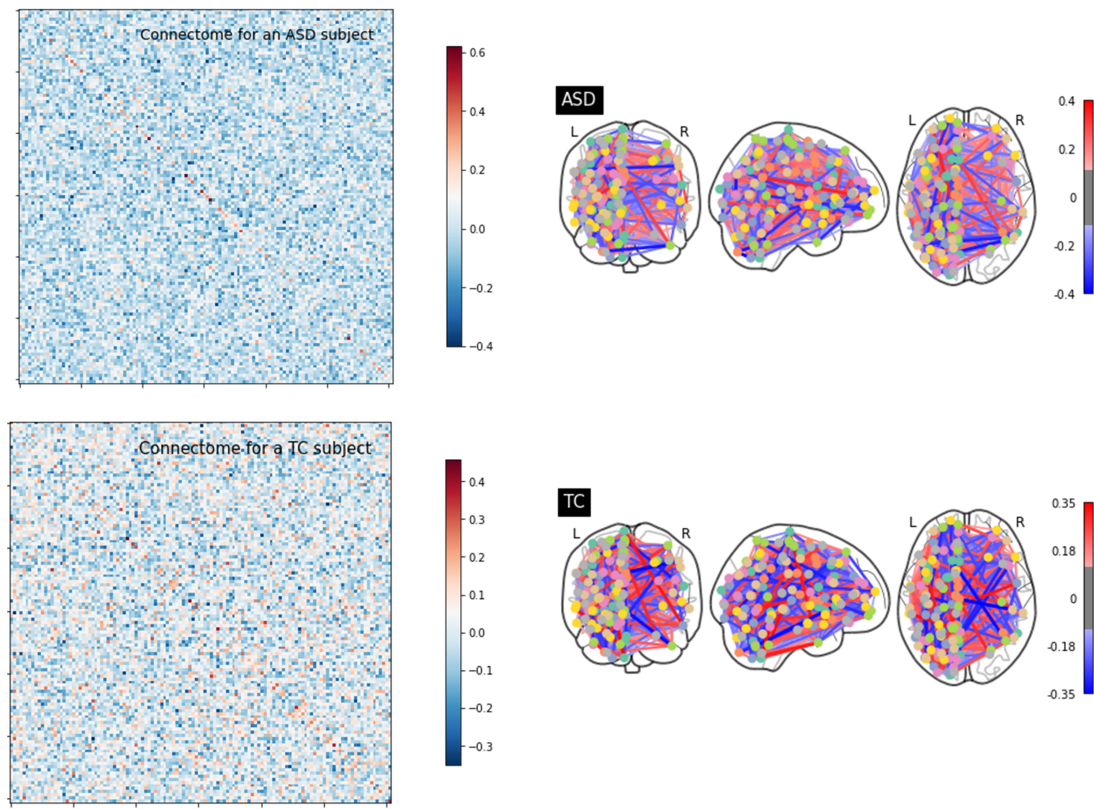


Figure 3.5: Difference between connectomes of random participants belonging to the ASD and control group.

The connectivity matrices were plotted using the `ConnectivityMeasure` function

belonging to the connectome class and the embedded connectome was created using the `view_connectome` function from the plotting class of Nilearn library.

3.3.4 Transforming 2D Functional Connectivity Matrix to 1D Feature Vector

The tangent connectivity matrix is symmetrical and the upper triangular value repeats the lower one. To reduce dimensionality, we remove the upper triangular value including the diagonal and retrieve the lower triangular value as shown in Figure 3.6. Next, the lower triangular part of interest is flattened to a 1D vector of size,

$$S = \frac{N(N - 1)}{2} \quad (3.1)$$

where N = number of ROIs. Thus, using the stated atlases, we received a feature vector of size 19,900, 6670, 7381, and 34,716, respectively, for CC200, AAL, BASC, and Power atlases in the case of each subject.

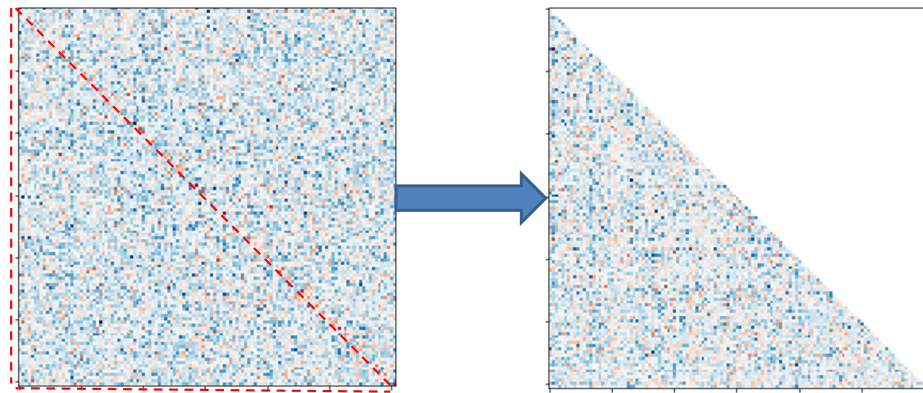


Figure 3.6: Retrieval of lower triangular part from symmetrical connectivity matrix.

3.3.5 Classification

Classification is the process of assigning an unknown sample to a pre-defined class or label after training the classifier on a set of training data. Performance of

machine learning classifiers such as KNN, Random Forest, Naïve Bayes, etc to successfully predict functional connectivity-based classification have been compared across rs-fMRI cohorts by Dadi et al. [54]. To our knowledge, no comparative analysis has been conducted using deep learning classifiers and multiple atlases to outline the impact of modelling choices on predicting over diverse phenotypes, as of now. Hence, in this study, we perform the classification task using a DNN (Deep Neural Network) classifier.

Deep neural networks, also termed as Feed-Forward Networks are supervised learning-based classifiers in which data flow is unidirectional from input to the output layer and consists of at least two hidden layers. The outputs are obtained by backpropagation. The backpropagation technique performs fine-tuning of the weights of a neural network to output the expected class minimizing prediction error. The hyperparameters involved in this classification are described in the following subsections along with their mathematical basis.

3.3.5.1 Hidden Layers and Number of Neurons

The obtained feature vectors were provided as input to the proposed deep neural network classifier (DNN). The proposed DNN (referred as Model-2 in the later sections) consisted of two hidden layers with 32 neurons per layer, as illustrated in Figure 3.7.

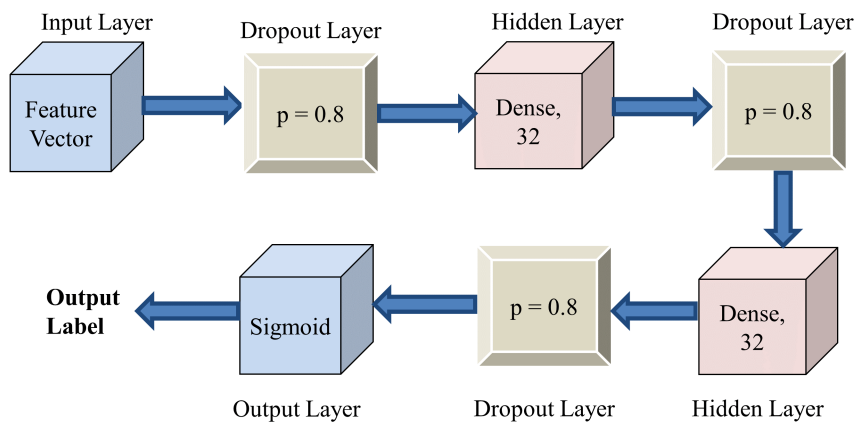


Figure 3.7: Proposed deep neural network architecture to predict ASD.

Other configurations with more than 2 hidden layers were also attempted but experimental results decreased due to lack of training samples.

3.3.5.2 Activation Function

Activation functions help the network learn complex patterns in the data and transforms the output of the network within a certain range which aids in making effective predictions. In this, network, the hidden layers use relu activation and the final output layer uses the sigmoid activation function.

Let, x_i and b_i be the input and bias value of layer i respectively, W_i is the weight vector connecting the nodes in layer i to the nodes in layer $i + 1$, then, layer $i + 1$ is activated using the following equation 3.2:

$$Z_{i+1} = f(W_i x_i + b_i) \quad (3.2)$$

where Z denotes activation of the subscripted hidden layer and f is the ReLU activation function defined in equation 3.3:

$$f(x) = \max(0, x) \quad (3.3)$$

In the case of sigmoid,

$$f(x) = \frac{1}{1 + e^{-x}} \quad (3.4)$$

where e = Euler's number. It exists between 0 and 1 and predicts the probability value as an output in the case of binary classification.

3.3.5.3 Optimizer

The function of an optimizer is to change attributes like weight and learning rate to reduce losses. Adam optimizer has been used in this regard with a relatively low learning rate of 0.0001. Adam is an adaptive learning rate optimization

algorithm which can be considered a combination of RMSProp and SGD with momentum.

3.3.5.4 Loss Function

The binary cross-entropy loss function is used in this binary classification problems (autism vs control). This loss function is defined in equation 3.5:

$$J = -\frac{1}{m} \sum_{i=1}^m [y_i \cdot \log(p(y_i)) + (1 - y_i) \cdot \log(p(1 - y_i))] \quad (3.5)$$

Where m is the total number of samples, y is the label and p indicates the probability of y belonging to autism or control group. The objective of the network is to minimize the value of loss function, J .

3.3.5.5 Regularizer

Since our input vector is high dimensional, we employed regularization techniques so that our model generalizes well, reduces the chance of overfitting and performs better on unseen data as well.

- **L2 Regularizer:** Also termed as weight decay, it updates the general cost function by adding another component or a regularized term to penalize large weights. Thus,

Cost Function = Binary cross-entropy loss + Regularization term

- **Dropout:** A dropout layer randomly selects some neurons/nodes and removes them at every iteration. Dropout layers with a dropout probability of 0.8 were used.

3.3.5.6 Batch Size

It refers to training samples utilized per iteration. A batch size of 10 has been used in this case. The reason for such a small batch size is to obtain a regularization effect and reduce generalization error.

3.3.5.7 Callback Functions

While training the neural network, we use the following Keras callback functions that enable us to interact with the process of training the model by providing a view of the internal states during training. The following callbacks were used.

- **Early Stopping:** The early stopping method allows us to choose a large random number of epochs while training. When the model performance stops improving on a validation set, training halts. This reduces the task of declaring a random number of epochs before training and fine-tuning it again and again. In this model, early stopping monitored validation loss with patience=5. If validation loss stopped decreasing after 5 consecutive epochs, training stops.
- **Model Checkpoint:** This function enables us to resume the training process in case of interruption and also use a pre-trained model without having to train it again by saving the model weights after every epoch. We set save_best_only = True, i.e, we save only the latest best weights while training the model by monitoring validation accuracy.

3.4 Conclusion

The methodology of our proposed deep learning-based procedure to identify ASD has been discussed in detail in this chapter. For extraction of time-series data, four standard predefined atlases were used. For functional connectivity computation, tangent space embedding was performed. The upcoming chapter contains detailed descriptions of the experimental result analyses on the proposed framework.

Chapter 4

Results and Discussions

4.1 Introduction

In the previous chapter, a detailed description of the overall autism spectrum disorder detection process and its various components were presented elaborately. The performance of the proposed method on the ABIDE dataset will be discussed in this chapter. Our main objective is to observe how our proposed model performs on unseen data and compute different performance metrics based on it.

This proposed method was implemented in Google Colab notebook using Python language. The training and testing of the model were carried out using Google Cloud provided backend free TPU runtime and 12.72 GB RAM on Intel Core i7 processor. It is most unfortunate that there exists no scope for collecting rs-fMRI scan data from health institutions in Chittagong due to the unavailability of such modern scan machines. Thus, for conducting this thesis, the dataset from the open-source multisite ABIDE repository was used.

4.2 Dataset Description

Experimental analysis was conducted over the ABIDE dataset. ABIDE is a consortium that has collected resting-state fMRI data and corresponding phenotypic information of subjects from 17 international sites [45]. Originally, it contained 1112 scans, including 539 ASD and 573 control individuals. However, all functional data could not pass the QAP (Quality Assessment Protocol) metrics as formulated by the PCP community [48], which reduced the size of the dataset to 866 subjects containing 402 ASD and 464 control subjects. Table 4.1 contains

the phenotypic information of the participants used in this study.

Table 4.1: Phenotypic information summary of the participants from the ABIDE dataset.

Autism Brain Imaging Data Exchange (ABIDE) Dataset				
Site	Count			Age Range
	ASD	Control	Total	
Caltech	5	10	15	17–56
CMU	6	4	10	19–40
KKI	12	20	32	8–13
LEUVEN	26	30	56	12–32
MAX_MUN	19	27	46	7–58
NYU	74	98	172	6–39
OHSU	12	13	25	8–15
OLIN	14	14	28	10–24
PITT	24	26	50	9–35
SBL	12	14	26	20–64
SDSU	8	18	26	9–17
Stanford	12	13	25	8–13
Trinity	19	25	44	12–26
UCLA	48	37	85	8–18
UM	46	73	119	8–29
USM	43	24	67	9–50
YALE	22	18	40	8–18
TOTAL	402	464	866	6–64

Detailed information about ABIDE dataset is available in [46].

4.3 Impact Analysis

The successful implementation of our research work regarding detection of autism spectrum disorder would result in a far-reaching impact in the present diagnosis process. Apart from the applications mentioned previously it would also pose a socio-environmental and ethical impact which are discussed below:

4.3.1 Social and Environmental Impact

The successful implementation of this method may be used for a wide range of applications, such as identifying neural activation patterns responsible for autism and performing visual evaluation of the functional characteristics of the autistic brain. By examining the contrast between the autistic and control brain, the underlying neural or biological basis of ASD can also be unveiled and established. Thus, creating a landmark in the medical diagnostic field.

4.3.2 Ethical Impact

Recent epidemiological investigations have confirmed a dramatic rise in the prevalence of ASD over the last several decades. Early diagnosis of ASD is indispensable to provide suitable rehabilitation of the patient at its earliest. It would obstruct the condition from degrading to a huge extent. But the existing subjective diagnosis process is less available than desired. Many clinics and health institutions do not possess expert clinicians or physicians eligible to conduct these extensive battery of behavioral assessments. Thus, many autistic children are not finally diagnosed until they get older. Such delay in diagnosis can be prevented to a great extent by the introduction of fMRI technique in autism detection.

4.4 Evaluation of Autism Spectrum Disorder Detection Framework

In this study, preprocessed 4D rs-fMRI data obtained from the ABIDE repository was subsequently converted to 1D feature vector passing through subsequent stages and provided to the deep neural network classifier for generating a prediction. After pre-processing, four different types of brain atlases were used to extract time-series data from pre-defined ROIs. A sample of time-series data extracted using BASC atlas comprising 122 ROIs is shown in Figure 4.1. It has a dimension of (196, 122) which refers to the average BOLD signal intensity measured from 122 brain regions at 196 different time-points.

```
Dimension: (196, 122)

[[ 0.04616885 -0.01526326  0.10384459 ... -0.04799895 -0.01127205
-0.00348043]
[-0.04603523  0.09968927 -0.54750889 ...  1.09339602 -0.8237821
-0.05795215]
[-0.03228574 -0.3025941   -1.50988694 ...   0.43313768 -1.77400955
0.10616049]
...
[ 0.03581149 -0.46697661  0.19506494 ...   0.17307072  1.15428784
0.1012403 ]
[-0.09814563 -0.40386377 -0.04761316 ...  -0.15362749  0.26044335
0.09486272]
[-0.10068468 -0.12794376  0.01533313 ...   0.04145647 -0.09778985
-0.16909604]]
```

Figure 4.1: Sample of mean time-series data from a random subject using BASC atlas.

From the aforementioned time-series data, functional connectivity measures or connectivity matrices were obtained using tangent space parametrization which converted the (196, 122) data to a matrix of dimension (122, 122). Finally, the lower half part of this matrix excluding the diagonal was retrieved and collapsed to form a 1D vector of dimension (7381,) as shown in Figure 4.2, since the remaining part of the matrix was redundant. These 1D feature vectors and corresponding class labels were provided as input to the classifier to get trained on and perform prediction tasks on the unseen test set.

Dimension: (7381,)

```
[ 2.20864799e-02  5.25763604e-02 -1.19500658e-01  8.95681658e-02
 6.23829464e-02  3.81589767e-02 -4.94229269e-02  8.20494892e-02
-2.71557872e-02 -1.72613311e-01  6.41120264e-04 -2.50656751e-02
-5.73590453e-02  2.86037840e-02 -2.09283606e-02 -1.44855642e-01
 9.24682177e-02 -1.59483240e-01  2.04132644e-01  1.05915110e-01
-1.06636051e-01 -1.41954283e-02 -1.87817160e-01 -2.70290380e-02
 9.28719512e-02 -2.78193410e-02  2.62654550e-02 -4.21671516e-02
-9.36487452e-02 -1.23044129e-02  5.50229903e-02 -3.24326747e-03
-8.03083759e-03 -5.28855967e-02 -1.27869943e-02 -1.13116730e-01
-1.71733496e-02 -8.84541201e-02  5.78677549e-02 -1.42252715e-02
-3.41463916e-02  2.24764692e-03 -5.42000824e-02  1.01279786e-01
-9.64965191e-02 -1.61728290e-01  3.02469136e-03  1.16437770e-01
-1.99205904e-02  1.56554536e-03 -2.22430768e-02  7.38622187e-02
-4.25402600e-02  7.12127662e-02 -2.66302909e-01 -5.68421900e-02
-5.50078481e-02 -4.27945037e-03 -9.28732035e-02 -2.08896374e-02
-4.54615068e-02  2.49563841e-02 -1.06033517e-01 -9.85540703e-03
-2.52162029e-02  6.40997932e-02  4.90703092e-02 -2.38967968e-02
-7.73935958e-02 -1.47454621e-01  5.10479613e-02  9.29942571e-02
 8.85713507e-02 -4.30609998e-02 -4.46146488e-02  1.43385775e-01
 3.60009177e-02  2.00277406e-02  4.68759103e-02 -1.07686872e-05
-6.53281453e-02  1.32605760e-01  4.06216241e-02  6.49042137e-03
 4.71967665e-02  9.87969977e-02  1.31970766e-01  6.49924206e-02
-1.02385655e-01 -4.71514647e-02 -1.03403038e-01  9.49953674e-03
-2.53970300e-02 -1.56022013e-02  5.65065611e-02 -1.09426973e-02
-3.59739066e-02  1.17435400e-01  3.16743696e-02 -6.16750784e-02
 8.90243740e-02  4.51709542e-02 -8.17935538e-02  2.81868653e-03
```

Figure 4.2: Sample of feature vector from a random subject using BASC atlas.

The entire classification task was performed using the Keras API with TensorFlow backend. For model evaluation, scoring strategy and numerical computation, the scikit learn library was used. To leverage the power of scikit learn tools while conducting model training and parameter tuning using Keras API, we used the

convenient Keras wrapper function known as KerasClassifier. The result of the prediction is shown in subsequent sections using a confusion matrix, different performance measures, plotting the AUC curve, and other performance charts.

4.5 Evaluation of Performance

For robust performance evaluation extensive fine-tuning and experimentation were performed in the DNN classifier by varying different hyperparameters. The number of hidden layer neurons of the deep neural network was varied within the range of 8 to 64, and performance was recorded in each case using each of the four atlases. The network structure represented in Figure 3.7 outperformed other configurations. Each network was validated using the stratified 5-fold cross-validation approach preserving the percentage of subjects in each target class (autism and control) to retain class balance. Twenty percent of the dataset was used as test cases, and the remaining 80% was utilized in training and validation. Within the training dataset, 80% of data was used for training and 20% for validation. A figurative representation of data partitioning is shown in Figure 4.3. This strategy allowed robust model evaluation while training and testing using different subsets of data.

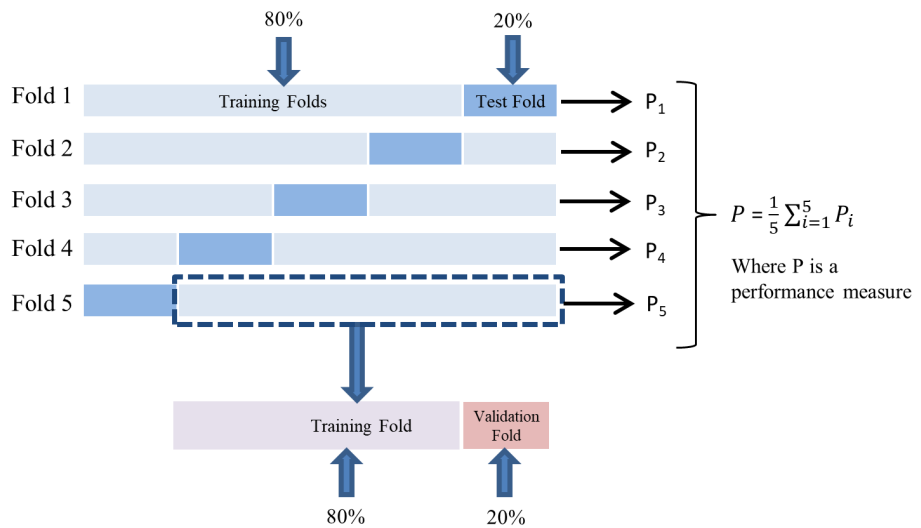


Figure 4.3: Data partitioning using stratified 5-fold cross-validation.

Apart from the most commonly used Accuracy metrics, we also measured our

model's performance using the confusion matrix and other terms associated with it to provide a better intuition of prediction results.

- **Confusion Matrix:** It is a 2x2 matrix for binary classification problems containing actual labels along one axis and predicted labels along the other axis as depicted in Figure 4.4

		Predicted Class	
		Positive Class	Negative Class
True Class	Positive Class	TP	FN
	Negative Class	FP	TN

Figure 4.4: Confusion Matrix.

1. **TP:** Positive labels that are correctly classified. In this case, correctly classified autistic subjects.
2. **TN:** Negative labels that are correctly classified, i.e, correctly classified control subjects.
3. **FP:** Actual negative labels that are incorrectly predicted to be positive, i.e, actual control subjects predicted as autistic subjects.
4. **FN:** Actual positive labels incorrectly predicted to be negative, i.e, autistic subjects that are predicted as control.

Using this set of values, the following performance metrics can be derived:

- $Accuracy = \frac{TP+TN}{TP+TN+FP+FN}$

- $Precision = \frac{TP}{TP+FP}$
- $Sensitivity = \frac{TP}{TP+FN}$
- $Specificity = \frac{TN}{TN+FP}$
- $F1 - Score = \frac{2*Precision*Recall}{Precision+Recall}$
- **AUC Curve:** The abbreviation for Area Under ROC (Receiver Operating Characteristic) Curve. It is a probability curve plotted with TPR (True Positive Rate) against FPR (False Positive Rate) which serves as a measure of separability between positive and negative labels. Higher the AUC, better the model in making correct predictions. AUC = 1 represents the best model performance.

In the following subsections, performance measures using each of the pre-defined atlases are depicted. Based on the parameters, training data are provided at each fold of the entire dataset then testing data is supplied for measuring model performance. Finally, an average performance measure of each metric for all 5 folds are calculated and represented.

4.5.1 Performance Evaluation Using Different Atlas

Mean performance metrics for different network configurations by fine-tuning using the mentioned atlases are represented in the following subsections. Tables ?? represent the value of sensitivity, F1-score, and AUC score for each atlas. Values of mean accuracy and its standard deviation are also shown in percentages. A dropout probability of 0.8 was introduced between each layer to control overfitting, as shown in Figure 3.7. All the models were compiled using the Adam optimizer with a learning rate of 0.0001 and binary cross-entropy loss function and trained with a batch size of 10. Confusion matrix and mean AUC (area under receiver operating characteristic curve) curves were also represented in each case.

4.5.1.1 CC200 Atlas

Analyzing the mean performance evaluation using five different network configurations from Table 4.2, it can be observed that CC200 achieved the highest accuracy and F1-score in our proposed Model-2. Though, sensitivity and AUC were the highest for Model-4. However, accuracy and F1 score were relatively lower. Model-2 achieved a relatively good score across all performance metrics. Figure 4.8 represents the confusion matrix and mean AUC curve using the proposed Model-2.

Table 4.2: Mean performance evaluation using Craddock 200 (CC200) atlas for different network configurations.

Model	Network Configuration			Mean Performance Evaluation using Craddock 200 (CC200) Atlas				
	Input Layer	Hidden Layer 1	Hidden Layer 2	Accuracy	Acc.Std (%)	Sensitivity	F1-Score	AUC Score
Model-1	19900	64	32	0.8473	1.57	0.9406	0.8510	0.9515
Model-2	19900	32	32	0.8668	2.38	0.8683	0.8579	0.9571
Model-3	19900	32	16	0.8530	3.02	0.7194	0.8185	0.9569
Model-4	19900	16	16	0.6843	2.74	0.9429	0.7343	0.9595
Model-5	19900	16	8	0.5947	4.23	0.9182	0.6770	0.9592

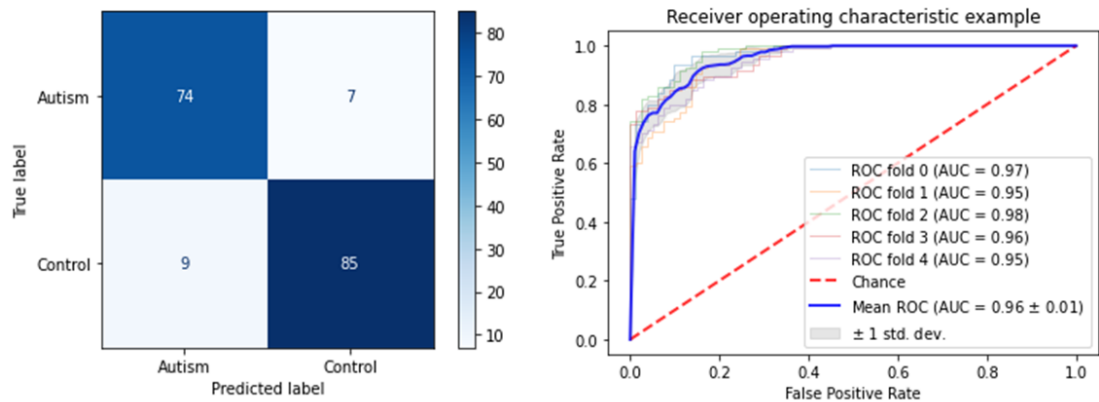


Figure 4.5: Confusion matrix and area under receiver operator characteristic curve (AUC) curve for CC200 atlas using Model-2.

4.5.1.2 Power Atlas

From Table 4.3, it is observed that the proposed Model-2 achieved a superior F1-score while the remaining scores were also greater than 85%. Model-5 obtained the highest sensitivity while accuracy and F1-score remained poor. AUC score remained almost constant at 95% for all models. Figure 4.6 represents the confusion matrix and mean AUC curve using the proposed Model-2.

Table 4.3: Mean performance evaluation using Power atlas for different network configurations.

Model	Network Configuration			Mean Performance Evaluation using Power Atlas				
	Input Layer	Hidden Layer 1	Hidden Layer 2	Accuracy	Acc.Std (%)	Sensitivity	F1-Score	AUC Score
Model-1	34716	64	32	0.7898	2.12	0.9626	0.8098	0.9513
Model-2	34716	32	32	0.8533	2.38	0.8633	0.8453	0.9531
Model-3	34716	32	16	0.8245	2.31	0.9429	0.8335	0.9505
Model-4	34716	16	16	0.8638	3.22	0.7662	0.8385	0.9565
Model-5	34716	16	8	0.5993	2.16	0.9802	0.6946	0.9509

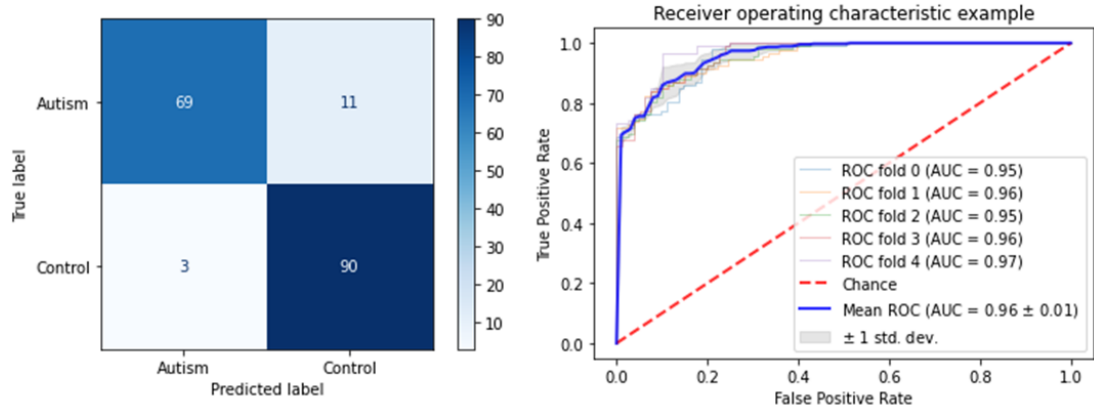


Figure 4.6: Confusion matrix and area under receiver operator characteristic curve (AUC) curve for Power atlas using Model-2.

4.5.1.3 BASC Atlas

Table 4.4 shows that the BASC atlas achieved the highest performance measure across all performance metrics using the proposed model. Figure 4.7 contains the confusion matrix and AUC curve using Model-2.

Table 4.4: Mean performance evaluation using BASC atlas for different network configurations.

Model	Network Configuration			Mean Performance Evaluation using Bootstrap Analysis of Stable Clusters (BASC) atlas				
	Input Layer	Hidden Layer 1	Hidden Layer 2	Accuracy	Acc.Std (%)	Sensitivity	F1-Score	AUC Score
Model-1	7381	64	32	0.8557	2.76	0.8634	0.8467	0.9570
Model-2	7381	32	32	0.8787	2.33	0.9029	0.8739	0.9587
Model-3	7381	32	16	0.8672	2.49	0.8507	0.8563	0.9439
Model-4	7381	16	16	0.8545	2.51	0.8358	0.8419	0.9471
Model-5	7381	16	8	0.8579	1.90	0.8731	0.8511	0.9418

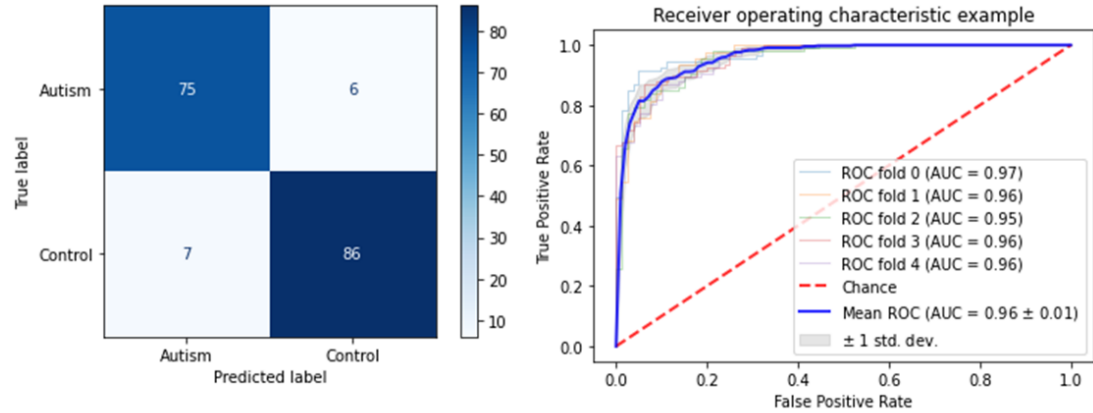


Figure 4.7: Confusion matrix and area under receiver operator characteristic curve (AUC) curve for BASC atlas using Model-2.

4.5.1.4 AAL Atlas

From Table 4.5, it is evident that AAL atlas represented a fluctuating performance across different models for each scoring metric. The confusion matrix and AUC curve using Model-2 are illustrated in Figure ??.

Table 4.5: Mean performance evaluation using AAL atlas for different network configurations.

Model	Network Configuration			Mean Performance Evaluation using Automated Anatomical Labeling (AAL) atlas				
	Input Layer	Hidden Layer 1	Hidden Layer 2	Accuracy	Acc.Std (%)	Sensitivity	F1-Score	AUC Score
Model-1	6670	64	32	0.8611	2.59	0.8933	0.8561	0.9523
Model-2	6670	32	32	0.8737	2.49	0.8412	0.8599	0.9512
Model-3	6670	32	16	0.8679	3.77	0.7941	0.8475	0.9500
Model-4	6670	16	16	0.8702	3.95	0.9082	0.8665	0.9522
Model-5	6670	16	8	0.8312	2.73	0.9404	0.8379	0.9509

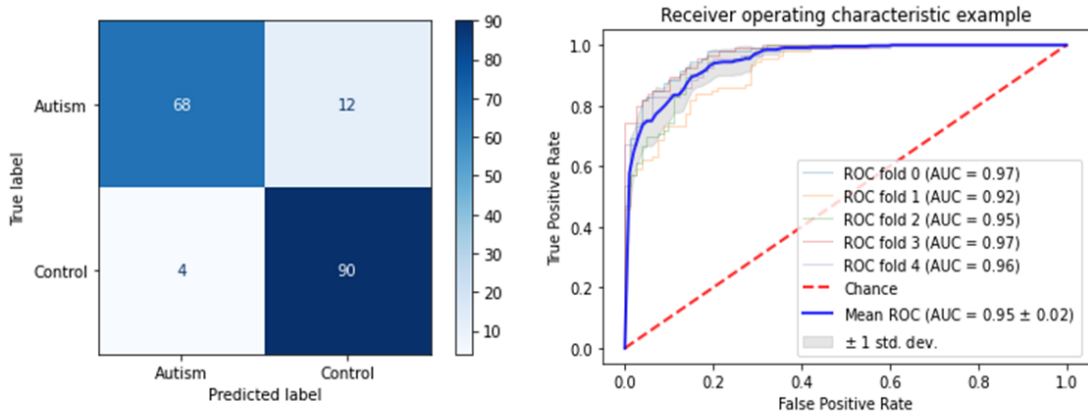


Figure 4.8: Confusion matrix and area under receiver operator characteristic curve (AUC) curve for AAL atlas using Model-2.

4.5.2 Performance Comparison among Atlases

A comparison of all performance metrics across all four atlases is represented in Figure 4.9 using the proposed Model-2 to determine which atlas had the most discriminative power in identifying autism and control cases.

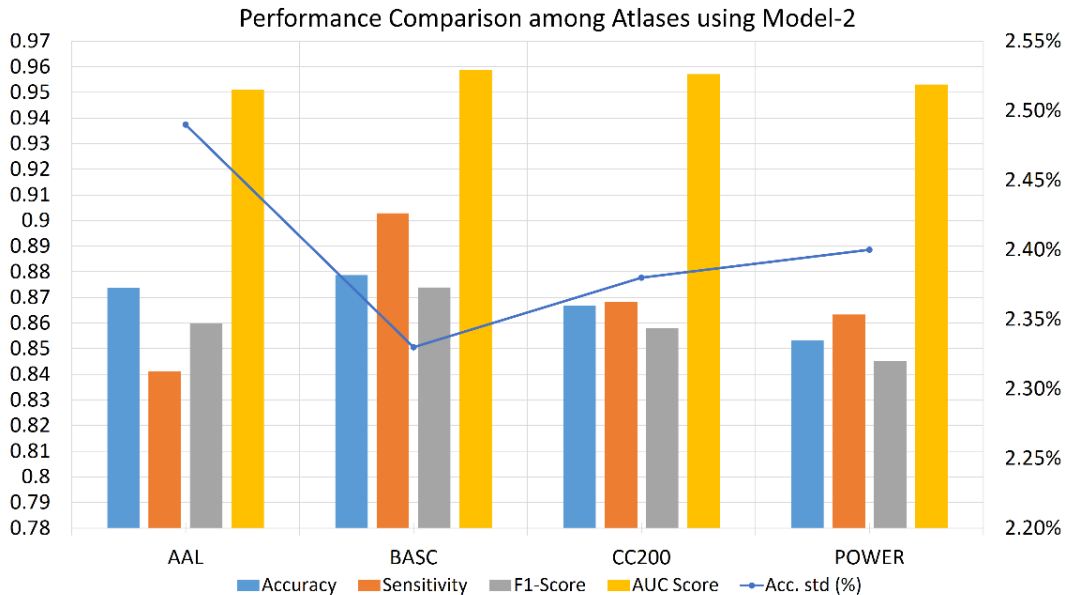


Figure 4.9: Performance comparison among atlases using Model-2.

From the above graphical analysis, the following points can be demonstrated:

- BASC atlas provided superior performance in terms of accuracy, sensitivity, F1, and AUC score using the proposed Model-2.
- AAL showed inconsistent results among various metrics. It had the lowest sensitivity value, which is very crucial and significant in medical diagnosis.
- CC200 and Power atlas depicted the lowest predictive power based on its performance value across all measures.
- The blue line chart depicts the standard deviation in percentage in terms of accuracy. BASC atlas has the least amount of deviation while AAL has maximum deviation.

From the aforementioned points, it can be concluded that the BASC atlas displays the best performance across all metrics. It exhibits the highest discriminative power in a balanced manner which is evident from its F1 score. Other models exceeding two hidden layers were also attempted, but experimental results deteriorated due to the limited dataset.

4.5.3 Performance Comparison Using BASC Atlas and Single-Site Data

A quantitative analysis of accuracy, sensitivity, and F1-score obtained by testing the proposed Model-2 classifier on data obtained from individual screening sites of ABIDE is represented in Table 4.6 using BASC atlas.

Table 4.6: Performance comparison using Model-2 and BASC atlas on data obtained from individual screening sites.

Site ID	No of Subjects	Accuracy	Sensitivity	F1-Score
PITT	50	0.94	0.96	0.94
YALE	40	0.95	0.91	0.95
NYU	172	0.92	0.92	0.91
UM	119	0.93	0.92	0.92

From the above tabular analysis, a significant improvement in performance can be observed across different performance metrics while using data obtained from individual screening sites. On the contrary, performance drops when the entire ABIDE dataset comprising 17 international sites was used for testing. This is

because different sites use different MRI acquisition protocols, scanning parameters, ways of laying the participants in the scanner, etc., which introduces huge variance across datasets obtained from different sites. Moreover, the effect of domain shift and distributional shift might also be responsible for such differences in performance measures.

4.5.4 Performance Comparison with Machine Learning Methods

Performance of machine learning classifiers, such as k-nearest neighbors (KNN), Random Forest, Naïve Bayes, etc., to successfully predict functional connectivity-based classification have been compared across rs-fMRI cohorts by Dadi et al. in [54]. To our knowledge, no such comparative analysis has been conducted using deep learning classifiers as of now. In Figure 4.10, a performance comparison between popular machine learning algorithms and our proposed Model-2 is represented. From this table, it is evident that our proposed deep learning model outperformed the machine learning techniques.

	L-SVM	KNN	DT	RF	GNB	Model-2
AAL	0.6613	0.481	0.5224	0.5637	0.6176	0.8737
BASC	0.6166	0.5473	0.5115	0.5427	0.62	0.8787
CC200	0.6865	0.5488	0.5166	0.574	0.6026	0.8668
POWER	0.6697	0.5265	0.5161	0.5254	0.6062	0.8533

Figure 4.10: Performance comparison with different machine learning algorithms.

Here, L-SVM indicates linear support vector machine; KNN means k-nearest neighbor; DT represents decision tree; RF indicates random forest and GNB means Gaussian Naïve Bayes classifier. Performance was measured using accuracy metrics. The Green–Yellow–Red color scale is used to highlight the performances where green indicates superior performance and red indicates the lowest performance.

4.5.5 Performance Comparison with Existing Literature

Table 4.7 illustrates the highest performance measure obtained from different existing works related to fMRI based ASD identification using brain atlases and our proposed model.

Table 4.7: Performance comparison with existing literature.

Methods	Year Published	Accuracy (%)
Heinsfeld et al. [10]	2018	70.00
Eslami et al. [41]	2019	70.30
Wang et al. [56]	2020	74.52
Yang et al. [57]	2020	75.27
Tang et al. [42]	2020	74.00
Our Proposed Model. [58]	2021	87.87

From above analysis it can be stated that the present study marked a significant performance improvement compared to existing studies. In our study, all the features extracted from the ROIs defined by each brain atlases were provided to the DNN classifier. Regardless of the size of the feature vector obtained after flattening of the functional connectivity matrix, no feature selection technique was used to select notable features while discarding the rest to reduce the risk of overfitting due to high dimensionality. In fact, dropout layers were introduced between each hidden layers to prevent overfitting. As such, all the features obtained from ROIs defined by the atlases (no matter how minimal or tremendous its effect might be in discriminating the two groups of participants) contributed to the ASD classification task which might be the reason for obtaining such an optimistic result. Besides, the use of suitable optimizer, weight initialization technique, learning rate, dropout rate, etc by fine-tuning also helps the neural network to extract meaningful information from the provided features that increases prediction accuracy compared to other methods that involved featured selection techniques.

4.6 Conclusion

This chapter provides the results of our proposed ASD detection framework and performs performance evaluation in multifarious ways. The comparative performances across different brain atlases, traditional machine learning methods and existing studies are also represented here. From all these perspective, our proposed framework using BASC atlas comprising 122 ROIs proved to be superior. The next chapter concludes this thesis and provides future recommendations.

Chapter 5

Conclusion

5.1 Conclusion

Earlier, in the field of automated diagnosis, ASD identification was questionnaire-based, parents interview-based, ADOS score or video gesture-based. Biswal et al. in [31] discovered that various brain regions still actively interact with each other while a subject was at rest (not in any cognitive task) in 1995. Then onwards, rs-fMRI has evolved as a noteworthy tool to explore brain networks by investigating local and global connectivity patterns and recent research has generated many invaluable insights regarding factors and brain regions that underlie brain. The primary goal of psychiatric neuroimaging research is to identify objective biomarkers that may inform the diagnosis and treatment of brain-based disorders. However, research works conducted using resting-state features for autism detection failed to reach biomarker standard till now.

In this paper, a deep learning approach using multisite resting-state fMRI was introduced to predict ASD. ASD detection is a challenging task since no standard modeling choice has yet been recognized, and the current practice is very much diverse. In this paper, preprocessed fMRI data were obtained from the CPAC pipeline. To extract mean BOLD signals from preprocessed data, brain atlases were used. A single brain atlas that can serve as a biomarker for the detection of ASD has not yet been discovered. Thus, four different standard and predefined atlases were used to extract ROIs. Connectivity matrices were prepared using tangent embedding and flattened to form a feature vector removing redundant information. This feature vector was provided as input to our proposed model.

Hidden layer configuration of the model was also varied, and its impact on detection observed. After performing a wide array of experiments, it has been confirmed that the BASC atlas using 122 ROIs yields higher predictive power than AAL, CC200, or Power atlases and can be considered to be more reliable in ASD diagnosis. It achieved 88% accuracy, 90% sensitivity, 87% F1-score, and 96% area under receiver operating characteristic curve. This result transcends most of the performances of existing works indicating that it is a promising method for ASD diagnosis.

5.2 Future Work

The present study marked a significant performance improvement compared to existing studies. Despite that, some limitations need to be addressed. Only functional MRI data were utilized here for classification, whereas a combination of functional and structural MRI data has proven to achieve high prediction accuracy in [43, 44]. Therefore, in future studies, other imaging modalities, such as structural MRI along with functional MRI data, may contain complementary information regarding ASD. However, implementation of the domain adaption technique [59] and encoding decoding technique [60] would also aid in prediction with more reliability and generalize well on unseen data obtained from different screening sites following different acquisition protocol. Other advanced neural network architectures, such as CNN, 3D based CNN model, etc., can also be utilized for prediction purposes and might prove to be fruitful. Furthermore, other options for implementing pipeline steps, such as usage of other available atlases, such as CC400, HO, Dosenbach, MSDL, etc., usage of first principal component-based time series extraction as in [61], non-correlation based functional connectivity matrix parametrization as in [62] and graph-based spectral method of vectorization as in [63], are aimed to be implemented in future studies.

References

- [1] M. Elsabbagh, G. Divan, Y.-J. Koh, Y. S. Kim, S. Kauchali, C. Marcin, C. Montiel-Nava, V. Patel, C. S. Paula, C. Wang *et al.*, ‘Global prevalence of autism and other pervasive developmental disorders,’ *Autism research*, vol. 5, no. 3, pp. 160–179, 2012 (cit. on p. 1).
- [2] *Autism spectrum disorders*. [Online]. Available: <https://www.who.int/news-room/fact-sheets/detail/autism-spectrum-disorders> (cit. on p. 1).
- [3] K. Gotham, A. Pickles and C. Lord, ‘Trajectories of autism severity in children using standardized ados scores,’ *Pediatrics*, vol. 130, no. 5, e1278–e1284, 2012 (cit. on p. 1).
- [4] P. Szatmari, S. Georgiades, E. Duku, T. A. Bennett, S. Bryson, E. Fombonne, P. Mirenda, W. Roberts, I. M. Smith, T. Vaillancourt *et al.*, ‘Developmental trajectories of symptom severity and adaptive functioning in an inception cohort of preschool children with autism spectrum disorder,’ *JAMA psychiatry*, vol. 72, no. 3, pp. 276–283, 2015 (cit. on p. 1).
- [5] C. Lord, M. Rutter, S. Goode, J. Heemsbergen, H. Jordan, L. Mawhood and E. Schopler, ‘Austism diagnostic observation schedule: A standardized observation of communicative and social behavior,’ *Journal of autism and developmental disorders*, vol. 19, no. 2, pp. 185–212, 1989 (cit. on p. 1).
- [6] C. Lord, M. Rutter and A. Le Couteur, ‘Autism diagnostic interview-revised: A revised version of a diagnostic interview for caregivers of individuals with possible pervasive developmental disorders,’ *Journal of autism and developmental disorders*, vol. 24, no. 5, pp. 659–685, 1994 (cit. on p. 1).
- [7] G. Varoquaux and R. C. Craddock, ‘Learning and comparing functional connectomes across subjects,’ *NeuroImage*, vol. 80, pp. 405–415, 2013 (cit. on p. 2).
- [8] A. Abraham, M. P. Milham, A. Di Martino, R. C. Craddock, D. Samaras, B. Thirion and G. Varoquaux, ‘Deriving reproducible biomarkers from multi-site resting-state data: An autism-based example,’ *NeuroImage*, vol. 147, pp. 736–745, 2017 (cit. on p. 4).
- [9] M. R. Arbabshirani, S. Plis, J. Sui and V. D. Calhoun, ‘Single subject prediction of brain disorders in neuroimaging: Promises and pitfalls,’ *Neuroimage*, vol. 145, pp. 137–165, 2017 (cit. on p. 4).
- [10] A. S. Heinsfeld, A. R. Franco, R. C. Craddock, A. Buchweitz and F. Meneguzzi, ‘Identification of autism spectrum disorder using deep learning and the abide dataset,’ *NeuroImage: Clinical*, vol. 17, pp. 16–23, 2018 (cit. on pp. 5, 13, 42).

- [11] M. Leo, P. Carcagni, C. Distante, P. L. Mazzeo, P. Spagnolo, A. Levante, S. Petrocchi and F. Lecciso, ‘Computational analysis of deep visual data for quantifying facial expression production,’ *Applied Sciences*, vol. 9, no. 21, p. 4542, 2019 (cit. on p. 8).
- [12] J. Han, Y. Li, J. Kang, E. Cai, Z. Tong, G. Ouyang and X. Li, ‘Global synchronization of multichannel eeg based on rényi entropy in children with autism spectrum disorder,’ *Applied Sciences*, vol. 7, no. 3, p. 257, 2017 (cit. on p. 8).
- [13] X. Liu, Q. Wu, W. Zhao and X. Luo, ‘Technology-facilitated diagnosis and treatment of individuals with autism spectrum disorder: An engineering perspective,’ *Applied Sciences*, vol. 7, no. 10, p. 1051, 2017 (cit. on p. 8).
- [14] D. Johnston, H. Egermann and G. Kearney, ‘Soundfields: A virtual reality game designed to address auditory hypersensitivity in individuals with autism spectrum disorder,’ *Applied Sciences*, vol. 10, no. 9, p. 2996, 2020 (cit. on p. 8).
- [15] ——, ‘Measuring the behavioral response to spatial audio within a multi-modal virtual reality environment in children with autism spectrum disorder,’ *Applied Sciences*, vol. 9, no. 15, p. 3152, 2019 (cit. on p. 8).
- [16] M. Magrini, O. Curzio, A. Carboni, D. Moroni, O. Salvetti and A. Melani, ‘Augmented interaction systems for supporting autistic children. evolution of a multichannel expressive tool: The semi project feasibility study,’ *Applied Sciences*, vol. 9, no. 15, p. 3081, 2019 (cit. on p. 8).
- [17] A. G. Garrity, G. D. Pearlson, K. McKiernan, D. Lloyd, K. A. Kiehl and V. D. Calhoun, ‘Aberrant “default mode” functional connectivity in schizophrenia,’ *American journal of psychiatry*, vol. 164, no. 3, pp. 450–457, 2007 (cit. on p. 8).
- [18] Y. Zhou, M. Liang, L. Tian, K. Wang, Y. Hao, H. Liu, Z. Liu and T. Jiang, ‘Functional disintegration in paranoid schizophrenia using resting-state fmri,’ *Schizophrenia research*, vol. 97, no. 1-3, pp. 194–205, 2007 (cit. on p. 8).
- [19] M. J. Jafri, G. D. Pearlson, M. Stevens and V. D. Calhoun, ‘A method for functional network connectivity among spatially independent resting-state components in schizophrenia,’ *Neuroimage*, vol. 39, no. 4, pp. 1666–1681, 2008 (cit. on p. 8).
- [20] V. D. Calhoun, J. Sui, K. Kiehl, J. A. Turner, E. A. Allen and G. Pearlson, ‘Exploring the psychosis functional connectome: Aberrant intrinsic networks in schizophrenia and bipolar disorder,’ *Frontiers in psychiatry*, vol. 2, p. 75, 2012 (cit. on p. 8).
- [21] R. C. Craddock, P. E. Holtzheimer III, X. P. Hu and H. S. Mayberg, ‘Disease state prediction from resting state functional connectivity,’ *Magnetic Resonance in Medicine: An Official Journal of the International Society for*

- Magnetic Resonance in Medicine*, vol. 62, no. 6, pp. 1619–1628, 2009 (cit. on p. 8).
- [22] M. Plitt, K. A. Barnes and A. Martin, ‘Functional connectivity classification of autism identifies highly predictive brain features but falls short of biomarker standards,’ *NeuroImage: Clinical*, vol. 7, pp. 359–366, 2015 (cit. on p. 8).
 - [23] J. S. Anderson, J. A. Nielsen, A. L. Froehlich, M. B. DuBray, T. J. Druzgal, A. N. Cariello, J. R. Cooperrider, B. A. Zielinski, C. Ravichandran, P. T. Fletcher *et al.*, ‘Functional connectivity magnetic resonance imaging classification of autism,’ *Brain*, vol. 134, no. 12, pp. 3742–3754, 2011 (cit. on p. 8).
 - [24] C. Shi, J. Zhang and X. Wu, ‘An fmri feature selection method based on a minimum spanning tree for identifying patients with autism,’ *Symmetry*, vol. 12, no. 12, p. 1995, 2020 (cit. on p. 8).
 - [25] Z. Rakhimberdina, X. Liu and T. Murata, ‘Population graph-based multi-model ensemble method for diagnosing autism spectrum disorder,’ *Sensors*, vol. 20, no. 21, p. 6001, 2020 (cit. on p. 8).
 - [26] T. Zhang, C. Li, P. Li, Y. Peng, X. Kang, C. Jiang, F. Li, X. Zhu, D. Yao, B. Biswal *et al.*, ‘Separated channel attention convolutional neural network (sc-cnn-attention) to identify adhd in multi-site rs-fmri dataset,’ *Entropy*, vol. 22, no. 8, p. 893, 2020 (cit. on p. 8).
 - [27] M. D. Greicius, G. Srivastava, A. L. Reiss and V. Menon, ‘Default-mode network activity distinguishes alzheimer’s disease from healthy aging: Evidence from functional mri,’ *Proceedings of the National Academy of Sciences*, vol. 101, no. 13, pp. 4637–4642, 2004 (cit. on p. 8).
 - [28] G. Chen, B. D. Ward, C. Xie, W. Li, Z. Wu, J. L. Jones, M. Franczak, P. Antuono and S.-J. Li, ‘Classification of alzheimer disease, mild cognitive impairment, and normal cognitive status with large-scale network analysis based on resting-state functional mr imaging,’ *Radiology*, vol. 259, no. 1, pp. 213–221, 2011 (cit. on p. 8).
 - [29] X. Guo, K. C. Dominick, A. A. Minai, H. Li, C. A. Erickson and L. J. Lu, ‘Diagnosing autism spectrum disorder from brain resting-state functional connectivity patterns using a deep neural network with a novel feature selection method,’ *Frontiers in neuroscience*, vol. 11, p. 460, 2017 (cit. on p. 9).
 - [30] *Magnetic resonance imaging*, Apr. 2021. [Online]. Available: https://en.wikipedia.org/wiki/Magnetic_resonance_imaging (cit. on p. 9).
 - [31] B. B. Biswal, ‘Resting state fmri: A personal history,’ *Neuroimage*, vol. 62, no. 2, pp. 938–944, 2012 (cit. on pp. 11, 44).
 - [32] K. Riddle, C. J. Cascio and N. D. Woodward, ‘Brain structure in autism: A voxel-based morphometry analysis of the autism brain imaging database

- exchange (abide),' *Brain imaging and behavior*, vol. 11, no. 2, pp. 541–551, 2017 (cit. on p. 11).
- [33] E. H. Aylward, N. J. Minshew, K. Field, B. Sparks and N. Singh, 'Effects of age on brain volume and head circumference in autism,' *Neurology*, vol. 59, no. 2, pp. 175–183, 2002 (cit. on p. 11).
- [34] S. J. Palmen, H. E. Hulshoff Pol, C. Kemner, H. G. Schnack, S. Durston, B. E. Lahuis, R. S. Kahn and H. Van Engeland, 'Increased gray-matter volume in medication-naïve high-functioning children with autism spectrum disorder,' *Psychological medicine*, vol. 35, no. 4, pp. 561–570, 2005 (cit. on p. 11).
- [35] E. Courchesne, K. Pierce, C. M. Schumann, E. Redcay, J. A. Buckwalter, D. P. Kennedy and J. Morgan, 'Mapping early brain development in autism,' *Neuron*, vol. 56, no. 2, pp. 399–413, 2007 (cit. on p. 11).
- [36] M. Herbert, D. Ziegler, C. Deutsch, L. O'brien, N. Lange, A. Bakardjiev, J. Hodgson, K. Adrien, S. Steele, N. Makris *et al.*, 'Dissociations of cerebral cortex, subcortical and cerebral white matter volumes in autistic boys,' *Brain*, vol. 126, no. 5, pp. 1182–1192, 2003 (cit. on p. 12).
- [37] R. J. Jou, N. Mateljevic, N. J. Minshew, M. S. Keshavan and A. Y. Hardan, 'Reduced central white matter volume in autism: Implications for long-range connectivity,' *Psychiatry and clinical neurosciences*, vol. 65, no. 1, pp. 98–101, 2011 (cit. on p. 12).
- [38] Y. Kong, J. Gao, Y. Xu, Y. Pan, J. Wang and J. Liu, 'Classification of autism spectrum disorder by combining brain connectivity and deep neural network classifier,' *Neurocomputing*, vol. 324, pp. 63–68, 2019 (cit. on p. 12).
- [39] B. Biswal, F. Zerrin Yetkin, V. M. Haughton and J. S. Hyde, 'Functional connectivity in the motor cortex of resting human brain using echo-planar mri,' *Magnetic resonance in medicine*, vol. 34, no. 4, pp. 537–541, 1995 (cit. on p. 12).
- [40] J. A. Nielsen, B. A. Zielinski, P. T. Fletcher, A. L. Alexander, N. Lange, E. D. Bigler, J. E. Lainhart and J. S. Anderson, 'Multisite functional connectivity mri classification of autism: Abide results,' *Frontiers in human neuroscience*, vol. 7, p. 599, 2013 (cit. on p. 13).
- [41] T. Eslami, V. Mirjalili, A. Fong, A. R. Laird and F. Saeed, 'Asd-diagnet: A hybrid learning approach for detection of autism spectrum disorder using fmri data,' *Frontiers in neuroinformatics*, vol. 13, p. 70, 2019 (cit. on pp. 13, 16, 42).
- [42] M. Tang, P. Kumar, H. Chen and A. Shrivastava, 'Deep multimodal learning for the diagnosis of autism spectrum disorder,' *Journal of Imaging*, vol. 6, no. 6, p. 47, 2020 (cit. on pp. 14, 42).
- [43] M. Rakić, M. Cabezas, K. Kushibar, A. Oliver and X. Lladó, 'Improving the detection of autism spectrum disorder by combining structural and

- functional mri information,’ *NeuroImage: Clinical*, vol. 25, p. 102 181, 2020 (cit. on pp. 14, 45).
- [44] C. Mellema, A. Treacher, K. Nguyen and A. Montillo, ‘Multiple deep learning architectures achieve superior performance diagnosing autism spectrum disorder using features previously extracted from structural and functional mri,’ in *2019 IEEE 16th International Symposium on Biomedical Imaging (ISBI 2019)*, IEEE, 2019, pp. 1891–1895 (cit. on pp. 15, 45).
- [45] A. Di Martino, C.-G. Yan, Q. Li, E. Denio, F. X. Castellanos, K. Alaerts, J. S. Anderson, M. Assaf, S. Y. Bookheimer, M. Dapretto *et al.*, ‘The autism brain imaging data exchange: Towards a large-scale evaluation of the intrinsic brain architecture in autism,’ *Molecular psychiatry*, vol. 19, no. 6, pp. 659–667, 2014 (cit. on pp. 18, 29).
- [46] *Autism brain imaging data exchange i abide i*. [Online]. Available: http://fcon_1000.projects.nitrc.org/indi/abide/abide_I.html (cit. on pp. 18, 30).
- [47] C. Craddock, Y. Benhajali, C. Chu, F. Chouinard, A. Evans, A. Jakab, B. S. Khundrakpam, J. D. Lewis, Q. Li, M. Milham *et al.*, ‘The neuro bureau preprocessing initiative: Open sharing of preprocessed neuroimaging data and derivatives,’ *Frontiers in Neuroinformatics*, vol. 7, 2013 (cit. on p. 18).
- [48] *Abide preprocessed*. [Online]. Available: <http://preprocessed-connectomes-project.org/abide/> (cit. on pp. 19, 22, 29).
- [49] N. Tzourio-Mazoyer, B. Landeau, D. Papathanassiou, F. Crivello, O. Etard, N. Delcroix, B. Mazoyer and M. Joliot, ‘Automated anatomical labeling of activations in spm using a macroscopic anatomical parcellation of the mni mri single-subject brain,’ *Neuroimage*, vol. 15, no. 1, pp. 273–289, 2002 (cit. on p. 20).
- [50] P. Bellec, P. Rosa-Neto, O. C. Lyttelton, H. Benali and A. C. Evans, ‘Multi-level bootstrap analysis of stable clusters in resting-state fmri,’ *Neuroimage*, vol. 51, no. 3, pp. 1126–1139, 2010 (cit. on p. 21).
- [51] R. C. Craddock, G. A. James, P. E. Holtzheimer III, X. P. Hu and H. S. Mayberg, ‘A whole brain fmri atlas generated via spatially constrained spectral clustering,’ *Human brain mapping*, vol. 33, no. 8, pp. 1914–1928, 2012 (cit. on p. 21).
- [52] J. D. Power, A. L. Cohen, S. M. Nelson, G. S. Wig, K. A. Barnes, J. A. Church, A. C. Vogel, T. O. Laumann, F. M. Miezin, B. L. Schlaggar *et al.*, ‘Functional network organization of the human brain,’ *Neuron*, vol. 72, no. 4, pp. 665–678, 2011 (cit. on p. 21).
- [53] *Nilearn*: [Online]. Available: <https://nilearn.github.io/> (cit. on pp. 21, 23).

- [54] K. Dadi, M. Rahim, A. Abraham, D. Chyzhyk, M. Milham, B. Thirion, G. Varoquaux, A. D. N. Initiative *et al.*, ‘Benchmarking functional connectome-based predictive models for resting-state fmri,’ *NeuroImage*, vol. 192, pp. 115–134, 2019 (cit. on pp. 22, 25, 41).
- [55] G. Varoquaux, F. Baronnet, A. Kleinschmidt, P. Fillard and B. Thirion, ‘Detection of brain functional-connectivity difference in post-stroke patients using group-level covariance modeling,’ *Medical Image Computing and Computer-Assisted Intervention – MICCAI 2010 Lecture Notes in Computer Science*, pp. 200–208, 2010. DOI: 10.1007/978-3-642-15705-9_25 (cit. on p. 23).
- [56] Y. Wang, J. Wang, F.-X. Wu, R. Hayrat and J. Liu, ‘Aimafe: Autism spectrum disorder identification with multi-atlas deep feature representation and ensemble learning,’ *Journal of Neuroscience Methods*, p. 108 840, 2020 (cit. on p. 42).
- [57] X. Yang, P. T. Schrader and N. Zhang, ‘A deep neural network study of the abide repository on autism spectrum classification,’ (cit. on p. 42).
- [58] F. Z. Subah, K. Deb, P. K. Dhar and T. Koshiba, ‘A deep learning approach to predict autism spectrum disorder using multisite resting-state fmri,’ *Applied Sciences*, vol. 11, no. 8, p. 3636, 2021 (cit. on p. 42).
- [59] X. Li, Y. Gu, N. Dvornek, L. H. Staib, P. Ventola and J. S. Duncan, ‘Multisite fmri analysis using privacy-preserving federated learning and domain adaptation: Abide results,’ *Medical Image Analysis*, vol. 65, p. 101 765, 2020. DOI: 10.1016/j.media.2020.101765 (cit. on p. 45).
- [60] C. Du, J. Li, L. Huang and H. He, ‘Brain encoding and decoding in fmri with bidirectional deep generative models,’ *Engineering*, vol. 5, no. 5, pp. 948–953, 2019 (cit. on p. 45).
- [61] W. Yassin, H. Nakatani, Y. Zhu, M. Kojima, K. Owada, H. Kuwabara, W. Gonoi, Y. Aoki, H. Takao, T. Natsubori *et al.*, ‘Machine-learning classification using neuroimaging data in schizophrenia, autism, ultra-high risk and first-episode psychosis,’ *Translational psychiatry*, vol. 10, no. 1, pp. 1–11, 2020 (cit. on p. 45).
- [62] M. Venkatesh, J. Jaja and L. Pessoa, ‘Comparing functional connectivity matrices: A geometry-aware approach applied to participant identification,’ *NeuroImage*, vol. 207, p. 116 398, 2020 (cit. on p. 45).
- [63] F. V. Farahani, W. Karwowski and N. R. Lighthall, ‘Application of graph theory for identifying connectivity patterns in human brain networks: A systematic review,’ *frontiers in Neuroscience*, vol. 13, p. 585, 2019 (cit. on p. 45).